

Katarzyna Natalia Jarzemska

*Department of Chemistry, University of Warsaw
Żwirki i Wigury 101, 02-089 Warsaw, Poland*



photocrystallography.eu

At the Intersection of Spectroscopy and Crystallography – Physicochemical Studies of Selected Photoactive Coordination Complexes



Załącznik nr 2b

Autoreferat w języku angielskim

Attachment No. 2b

Self-presentation in English

Warsaw, March 2019

TABLE OF CONTENTS

1. PERSONAL AND CONTACT DATA	3
2. DIPLOMA AND SCIENTIFIC DEGREES.....	3
3. EMPLOYMENT RECORD	3
4. INDICATION OF THE SCIENTIFIC ACHIEVEMENT	4
4.1. Title of the scientific achievement.....	4
4.2. List of publications constituting the scientific achievement.....	4
4.3. Description of the aim and results of the scientific achievement.....	8
4.3.1. Introduction and motivation	8
4.3.2. New luminescent boron complexes – synthesis, structure and spectroscopy	9
4.3.3. Transition-metal complexes – structure, spectroscopy, photoelectrochemistry [...].	26
4.3.4. Summary	41
4.3.5. Research plans for the next few years.....	42
4.3.6. References.....	43
5. LIST OF THE REMAINING SCIENTIFIC PUBLICATIONS.....	49

1. Personal and contact data

Names and surname: **Katarzyna Natalia Jarzemska**

Birth date and place: **1984, Warsaw, Poland**

E-mail address: katarzyna.jarzemska@gmail.com, katarzyna.jarzemska@uw.edu.pl

Website: www.photocrystallography.eu

2. Diploma and scientific degrees

- **2012: Doctor of Philosophy (chemical sciences)** – Department of Chemistry, University of Warsaw, Warsaw, Poland

Title of the PhD thesis: *“Extension of the aspherical pseudoatom databank towards nucleic acids and its application in structural, charge density and energy studies”*ⁱ (defended 12th October 2012, *summa cum laude*, supervisor: Prof. K. Woźniak, supporting supervisor: Dr. P. M. Dominiak).

- **2009: Post-graduate diploma** – Warsaw School of Economics, Warsaw, Poland

Post-graduate Studies on European Financial-Economic-Legal Relations (1-year course). Title of the thesis: *“Operational risk in credit institutions”*ⁱⁱ (very good grade, supervisor: Dr. W. Bołkunow).

- **2007: Master of Science (chemistry)** – College of Inter-Faculty Individual Studies in Mathematics and Natural Sciences, University of Warsaw, Warsaw, Poland

Title of the MSc thesis: *“Structural and spectroscopic properties of a series of ruthenium metathesis catalysts”*ⁱ (defended 30th May 2007, *summa cum laude*, supervisor: prof. K. Woźniak).

3. Employment record

- **2015 – present: Senior research associate** – Department of Chemistry, University of Warsaw, Warsaw, Poland

January–May 2017 and June–December 2018 – maternity leaves.

- **2013 – 2014: Postdoctoral research associate** – Department of Chemistry, University at Buffalo, The State University of New York, Buffalo, New York, United States

Post-doctoral stay in Prof. P. Coppens’ group was funded by the Polish Ministry of Science and Higher Education within the „Mobility Plus” programme.

- **2013 – 2015: Research assistant** – Department of Chemistry, University of Warsaw, Warsaw, Poland

- **2012: Research technician** (part-time) – Department of Chemistry, University of Warsaw, Warsaw, Poland

ⁱ Thesis was entirely written in English.

ⁱⁱ Thesis was written in Polish. Original title: *“Ryzyko operacyjne w instytucjach kredytowych”*.

4. Indication of the scientific achievement ⁱⁱⁱ

4.1. Title of the scientific achievement

At the intersection of spectroscopy and crystallography – physico-chemical studies of selected photoactive coordination complexes

4.2. List of publications constituting the scientific achievement

An asterisk (*) indicates the corresponding author; the impact factor (IF) is given as in the year 2017 (the latest IF available in the Web of Science database); the number of citations (n.cit.) was taken from the Web of Science database (dated 6th March 2019); for each publication the initials of the names and surnames of the authors, the title of the work, the full name of the journal, publication year, volume number, page numbers and digital object identifier (DOI) are given; publications were grouped chronologically and thematically (see section 4.3).

- H1.** K. Durka,* **K. N. Jarzemska,*** R. Kamiński, S. Luliński, J. Serwatowski, K. Woźniak, “Nanotubular hydrogen-bonded organic framework architecture of 1,2-phenylenediboronic acid hosting ice clusters”, *Crystal Growth & Design*, **2013**, *13*, 4181–4185 (DOI: 10.1021/cg401087j).

(IF₂₀₁₇ = 3.972; n.cit. = 22)

My contribution included application of TAAM refinement to the crystal structures of ortho-phenylenediboronic acid determined earlier by co-author K. Durka, as well as planning and elaboration of the computational part of the paper. I carried out a series of periodic calculations for the studied crystal forms of ortho-phenylenediboronic acid. I modelled the distribution of water molecules inside the nanotubes built of acid molecules bound together by the hydrogen bonds. I found an analogy between water polymers that could be present inside the tubes and the structures of hexagonal and trigonal ice. I studied the effect of the solvent on the stability of the crystal lattice. I actively participated in the interpretation of results and writing of the manuscript. I wrote approximately half of the manuscript and performed the linguistic correction of the entire text. Together with K. Durka I am the corresponding author of the article, thus I actively participated in replying to the reviewers' comments. I estimate my contribution to this work as ca. 30%.

- H2.** **K. N. Jarzemska,*** R. Kamiński, K. Durka, M. Kubsik, K. Nawara, E. Witkowska, M. Wiloch, S. Luliński, J. Waluk, I. Głowacki, K. Woźniak, “New class of easily-synthesisable and modifiable organic materials for applications in luminescent devices”, *Dyes and Pigments* **2017**, *138*, 267–277 (DOI: 10.1016/j.dyepig.2016.11.039).

(IF₂₀₁₇ = 3.767; n.cit. = 4)

My contribution included proposing the subject of the research/indication of the subject, the first synthesis of a model luminescent complex, planning and coordination of the entire study on the properties of the designed and synthesised series of systems based on fluorinated ortho-phenylenediboronic acids and 8-hydroxyquinoline. I developed the whole structural part, conducted all theoretical computations, interpreted and co-analysed all remaining results. I prepared the manuscript, occasionally making use of fragments received from the co-authors. I am the only corresponding author of the article, and submitted the manuscript to the journal and corresponded with the editor at the review stage. I estimate my contribution to this work as ca. 50%.

ⁱⁱⁱ According to Art. 16, item 2, Act of 14 March 2003 – Law on Higher Education, the Law on Academic Degrees and Title and Degrees in Art (Journal of Laws No 65, item 595 with further amendments).

- H3. K. N. Jarzemska,*** R. Kamiński, K. Durka, M. Kubsik, “Engineering of solvatomorphs of the luminescent complex of *ortho*-phenylenediboronic acid and 8-hydroxyquinoline”, *Crystal Growth & Design*, **2017**, *17*, 6836–6851 (DOI: 10.1021/acs.cgd.7b01420).

(IF₂₀₁₇ = 3.972; n.cit. = 2)

My contribution included formulation of the research topic, planning and coordination of the studies. I participated in the synthesis and crystallisation of the studied complexes. I performed and supervised structural measurements of the analysed solvatomorphs. Performed all theoretical computations presented in the article, as well as the luminescence measurements for the single-crystal samples. Summarised and analysed all results and wrote the whole manuscript. I am the only corresponding author of the article, and submitted the manuscript to the journal and corresponded with the editor at the review stage. I estimate my contribution to this work as ca. 70%.

- H4. K. N. Jarzemska,*** R. Kamiński, K. Durka, K. Woźniak, “Ground-state charge-density distribution in a crystal of the luminescent *ortho*-phenylenediboronic acid complex with 8-hydroxyquinoline”, *Journal of Physical Chemistry A*, **2018**, *122*, 4508–4520 (DOI: 10.1021/acs.jpca.8b00832).

(IF₂₀₁₇ = 2.836; n.cit. = 0)

My contribution included indicating of the research subject, as well as planning, coordinating and documenting of the research. I participated in the high-resolution X-ray diffraction measurement. Together with one of the co-authors conducted the data reduction. I carried out the multipole refinement and analysed the electron density distribution in the crystal. Performed all theoretical computations described in the article. Summarised, analysed and described all the results and wrote the whole manuscript. I am the only corresponding author of the article, and submitted the manuscript to the journal and corresponded with the editor at the review stage. I estimate my contribution to this work as ca. 70%.

- H5. S. E. Kutniewska, K. N. Jarzemska,*** R. Kamiński, A. J. Stasyuk, D. T. Gryko, M. K. Cyrański, “Structural, energetic and spectroscopic studies of new luminescent complexes based on 2-(2'-hydroxyphenyl)imidazo[1,2-*a*]pyridines and 1,2-phenylenediboronic acid”, *Acta Crystallographica Section B*, **2018**, *74*, 725–737 (DOI: 10.1107/S2052520618015469).

(IF₂₀₁₇ = 6.467; n.cit. = 0)

My contribution included indicating of the research subject, planning and coordinating of the research. Under my supervision, PhD student S. E. Kutniewska carried out syntheses and crystallisations of the designed luminescent systems, and followed with the collection of the UV-Vis absorption and luminescence spectra in the solution. Together with the co-authors I worked out the structural data and performed all theoretical computations for the purpose of the article. I analysed all collected data and prepared the whole manuscript. I am the only corresponding author of the article, and submitted the manuscript to the journal and corresponded with the editor at the review stage. I estimate my contribution to this work as ca. 45%.

- H6. K. N. Jarzemska,** Y. Chen, J. Nasca, E. Trzop, D. F. Watson, P. Coppens,* “Relating structure and photoelectrochemical properties: electron injection by structurally and theoretically characterized transition metal-doped phenanthroline-polioxotitanate nanoparticles”, *Physical Chemistry Chemical Physics*, **2014**, *16*, 15792–15795 (DOI: 10.1039/C4CP02509A).

(IF₂₀₁₇ = 3.906; n.cit. = 11)

My contribution included the X-ray diffraction measurements and structure determination of the studied compound, conducting all theoretical computations, as well as the design and construction of the photovoltaic cell. I participated in all photoelectrochemical measurements of the photocurrent (as a part of the established cooperation) generated by light irradiation of the studied polyoxotitanate cluster molecules. I analysed the collected data, prepared the first version of the manuscript (I wrote the majority of the text and prepared all the drawings), as well as participated in the discussions on its final version. I actively participated in formulating replies to the reviewers' comments. I estimate my contribution to this work as ca. 60%.

- H7. K. N. Jarzemska,*** R. Kamiński, B. Fournier, E. Trzop, J. D. Sokolow, R. Henning, Y. Chen, P. Coppens,* “Shedding light on the photochemistry of coinage-metal phosphorescent materials: a time-resolved Laue diffraction study of an Ag^I-Cu^I tetranuclear complex”, *Inorganic Chemistry*, **2014**, 53, 10594–10601 (DOI: 10.1021/ic501696y).

(IF₂₀₁₇ = 4.700; n.cit. = 13)

My contribution included work plan preparation and discussions aimed at selecting the most appropriate system for further photocrystallographic studies (based on a literature report prepared by a PhD student). I participated in the time-resolved synchrotron experiments and data reduction. I carried out the final refinement of the excited-state structure using the LASER program and analysed the result. Conducted all theoretical computations presented in the article, in particular the QM/MM modelling performed in order to determine the theoretical structure of the excited state. Summarized and analysed all results, as well as wrote the first version of the manuscript, which was then discussed and refined together with P. Coppens. I am (together with P. Coppens) the corresponding author of the article and I actively participated in phrasing replies to the reviewers' comments. I estimate my contribution to this work as ca. 50%.

- H8. K. N. Jarzemska,*** R. Kamiński, K. F. Dziubek, M. Citroni, D. Paliwoda, K. Durka, S. Fanetti, R. Bini, “Impact of high pressure on metallophilic interactions and its consequences for spectroscopic properties of a model tetranuclear silver(I)-copper(I) complex in the solid state”, *Inorganic Chemistry*, **2018**, 57, 8509–8520 (DOI: 10.1021/acs.inorgchem.8b01196).

(IF₂₀₁₇ = 4.700; n.cit. = 0)

My contribution included indicating of the research subject, planning, organising and coordinating the studies. This contribution is a continuation of my previous article devoted to the silver-copper complex. My idea was to examine the structure-spectroscopy properties depending on the applied (high) pressure. For this purpose, I successfully applied for the possibility of conducting research within the Laserlab-Europe consortium (LENS facility, Italy) and at the ESRF synchrotron (France). I took part in all experiments described in the article and coordinated them. I participated in the analysis of both high-pressure spectroscopic and structural data. Carried out all theoretical computations described in the article, as well as additional structural analyses. I wrote the manuscript, occasionally using fragments prepared by the co-authors. I am the only corresponding author of the article, and submitted the manuscript to the journal, and corresponded with the editor at the review stage. I estimate my contribution to this work as ca. 60%.

- H9. K. N. Jarzemska,*** M. Hapka, R. Kamiński, W. Bury, S. E. Kutniewska, D. Szarejko, M. M. Szcześniak, “On the nature of luminescence thermochromism of multinuclear copper(I) benzoate complexes in the crystalline state”, *Crystals*, **2019**, 9, 36 (DOI: 10.3390/cryst9010036).

(IF₂₀₁₇ = 2.144; n.cit. = 0)

Special issue entitled “Photocrystallography and Solid-State Structural Dynamics”

My contribution included indicating of the research subject, planning, organising and coordinating the studies. I performed a part of the X-ray diffraction experiments at various temperatures and developed the results. I carried out all luminescence measurements for both compounds in the solid state at different temperatures. I managed time-resolved synchrotron measurements (as part of my research project) and participated in processing the data. I interpreted and described the results in the form of a manuscript, using the computational part written initially by M. Hapka. I am the only corresponding author of the article, and submitted the manuscript to the journal and corresponded with the editor at the review stage. I estimate my contribution to this work as ca. 50%.

Scientometric data of the above contributions: ^{iv}

No. of research publications: **9**

Total number of citations (without self-citations): **52 (41)**

Total impact factor (IF): **36.464 (4.795** average per paper)

^{iv} According to the ISI Web of Science database on the 6th March 2019.

4.3. Description of the aim and results of the scientific achievement

4.3.1. Introduction and motivation

One of currently most important areas in chemistry is the development of new materials that respond rapidly and reliably to an external stimulus, and send out signals which provide specific information that may be further utilised. In this respect the investigations and understanding of charge transfer processes, occurring within and between molecules, and related phenomena, are among most challenging issues of modern science. In the long term such knowledge will enable us to control properties relevant for specific applications across all the size scales from molecules to bulk materials, which consequently will contribute to rational design of new functional materials, or to the development of innovative technological solutions.

In this view, photoactive materials constitute an interesting group of systems. This is because processes, such as, light-induced charge transfer from one part of a molecule to another, can result in energy conversion into the work used, amongst others in photoelectrochemical cells (*e.g.* DSSCs – dye-sensitized solar cells [1], or DSPECs – dye-sensitized photoelectro-synthesis cells [2]), or into light emission in diodes [3]. It is particularly important to study this type of phenomena occurring in solid materials due to their growing use in various areas of life. Direction of technological development clearly shows that solid-state chemistry and physics become science of the future. In turn, the crystalline phase definitely stands out among solid phases of matter. It is very well-defined and its structure can be determined using X-ray diffraction methods. The possibility of tracking structural changes via crystallographic approaches, and thus, of further determination of the 3-dimensional structure of all individuals (*e.g.* electronic excited states) inside the crystal, is of great significance in the pursuit of gaining full understanding of processes occurring during the excitation of molecules. Therefore crystals are ideal model systems for studying processes which take place when a sample is subjected to an external stimulus (*e.g.* a light pulse).

The challenges described above and the fact that I am a crystallographer by education, have become the inspiration for the research undertaken after obtaining a doctoral degree. I have decided to combine the acquired crystallographic skills with spectroscopic and computational chemistry methods in order to solve interesting and significant problems of science, going as far as possible beyond routine structural measurements. My previous efforts dedicated to study and design of functional photoactive materials resulted, among others, in a series of nine contributions which I selected [H1-H9], as the basis of my habilitation application. The outcomes included in my habilitation achievement, which I present here in a synthetic way, can be divided into two parts with a clearly defined common ground – the research objects are crystals of photoactive complexes, while the applied research methods oscillate mainly between crystallography and spectroscopy, approaching photocystallography.¹ The first group of articles concerns a new class of luminescent organoboron compounds [H1-H5], while the second group contains articles devoted to light-induced charge transfer processes in crystals of selected transition-metal complexes examined under various conditions [H6-H9]. I have decided to combine both groups of articles for a more comprehensive presentation of current research possibilities, with particular emphasis on advanced photocystallographic methods, which are better suited for materials containing atoms of heavier elements. Furthermore, I considered that all these publications show in a very lucid way the development of my skills as a scientist, from

¹ It is worth noting that it was possible to conduct the presented research – especially spectroscopic and photocystallographic experiments – thanks to the „Mobility Plus” postdoctoral fellowship (Ministry of Science and Higher Education) and SONATA research grant (National Science Centre).

the completion of my doctorate, through an extremely fruitful period of postdoctoral internship, until independent academic work, which I currently conduct at the University of Warsaw.

4.3.2. New luminescent boron complexes – synthesis, structure and spectroscopy

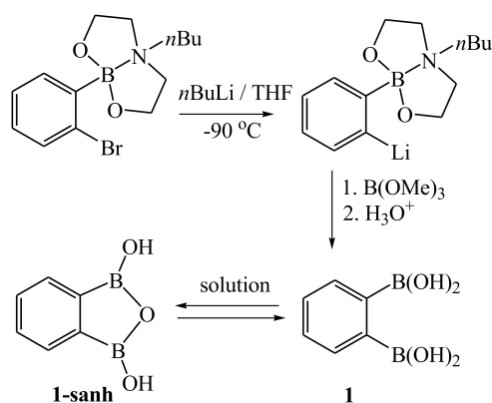
As mentioned above, the first group of articles constituting my habilitation achievement that shall be presented further on, concerns the photoactive organoboron systems, *i.e.* compounds containing a boron atom bound directly to a carbon atom. The most important classes of such compounds involve systems containing a 3-coordinated boron atom in their molecular structures, *e.g.*, organoboronic acids ($R-B(OH)_2$, R = organic substituent), diorganoboronic acids (R_2B-OH), or triorganoborates (R_3B) and their derivatives. Particularly noteworthy is the first, widest group of compounds, *i.e.* boronic acids, which are non-toxic and easily degradable in the natural environment [4]. Boronic acids also include a wide range of important applications, such as in organic synthesis (*e.g.* the famous Suzuki-Miyaura reaction) [5-6], analytical chemistry (determination of sugar concentration, construction of sensors sensitive to the presence of selected anions, *etc.*) [7-12], or even medicine (cancer therapy BNCT, boron-neutron capture therapy; some compounds exhibit antibacterial, antifungal, or anticancer activity) [13-20]. Among this group arylboronic derivatives are especially interesting, being generally more stable and not undergoing hydrolysis [4]. Furthermore, such compounds are readily applied in the field of crystal engineering thanks to their similarity to aromatic carboxylic acids and simultaneously their greater functionalisation potential than that of the latter systems (boronic group – $B(OH)_2$ – is capable of forming a greater number of hydrogen bonds as compared to the carboxylic function – CO_2H). Because of their stability and non-toxicity, boronic acids, alike their carboxylic analogues, may be used as auxiliary substances in pharmaceuticals, namely as components of cocrystals accompanying the so-called active pharmaceutical ingredients (APIs) [21-22]. The most important application of such substances concerns modification of the drug solubility, which affects its pharmacokinetics in the body and, for example, accelerates the action of the active substance, or allows the use of different drug doses [23].

In the context of my habilitation achievement, I would also like to point out here the remarkable luminescent properties that some classes of boron compounds exhibit. One of the first photoactive boron coordination complexes was designed following the example of previously known luminescent aluminium systems (*e.g.* AlQ_3 , Q = 8-oxyquinolato ligand) [24]. The advantage of boron compounds over aluminium analogues is their greater stability, which facilitates practical applications. For this reason the interest in luminescent boron complexes has grown significantly, thus over the last few years a lot of photoactive organoboron systems have been synthesised. Among this group of compounds, worth mentioning are boronic complexes [25-28]. This kind of systems have already been successfully used, for example, in construction of *n*-type semiconductors [29-30] or in luminescent polymers [31-34]. Furthermore, they often exhibit relatively high emission quantum yields, such as approximately 39% for the boronic system containing the 8-oxyquinolato ligand [28], about 38% in the case of systems based on the 2,2'-biphenyl core [35], or as much as about 63% for the 9,10-diborantracene complexes [27].

At the beginning, in cooperation with my colleague Krzysztof Durka from the Warsaw University of Technology, I have studied the boron compounds regarding their crystal structures, crystal network stability and formed structural motifs [**P11**,**P25**,**P31**]. Our first joint publication [**P31**] was dedicated to *para*-phenylenediboronic acid ($(HO)_2B-C_6H_4-B(OH)_2$) and its fluorine derivatives. At this point it is worth noting the analysed parent *para*-

phenylenediboronic acid. It exists in two known crystalline forms of $P\bar{1}$ space group symmetry – an anhydrous form and a hydrate containing 4 molecules of water per 1 acid molecule. In both of these crystal structures, the acid dimer stabilised by hydrogen bonds formed between boronic groups constitutes the main structural motif. There are also significant stacking interactions between aromatic acid fragments and boronic groups encountered in both cases, while the lateral interactions between boronic groups in the anhydrous form are replaced by the acid···water interactions in the hydrate. Water molecules in the latter crystal form are arranged in molecular layers parallel to the (010) crystal planes and stabilised by hydrogen bonds, by means of which water species also interact with the adjacent acid molecules leading to a 3-dimensional network. In turn, the isomeric *meta*-phenylenediboronic acid crystallises in the $C2/c$ space group, with half of the molecule in the asymmetric unit (ASU) [36]. Until now it is the only known crystal form of this compound. In this case the main structural motifs are very similar in nature to those observed in the anhydrous form of *para*-phenylenediboronic acid. Through our studies, it also turned out that *para*-phenylenediboronic acid readily co-crystallises with other compounds, such as aromatic *N*-oxides, as described in one of our papers [P7]. We have also conducted co-crystallisations of both isomeric acids with simple pharmaceuticals, and the *para* compound appeared to form more willingly such systems than the *meta* isomer. These results are currently being prepared for publication.

[H1] **Cryst. Growth Des.**, 2013, 13, 4181. Synthesis and similar analysis of *ortho*-phenylenediboronic acid (**odba**) constituted a natural continuation of the described research, and, as it turned out later, was the beginning of an interesting scientific adventure. The compound was obtained by K. Durka, who employed an ingenious method developed earlier by his PhD supervisor, Sergiusz Luliński (Scheme 1). The successful synthesis was itself a very important outcome, whereas **odba** crystallisation provided further more interesting research topics. It appeared that **odba** may exist in three crystal forms, which differ by crystal packing and solvent content. Such variety of crystal structures allowed for drawing general conclusions on relative stability of the examined crystal structures depending on the presence and amount of solvent. The particularly interesting trigonal form, in which acid molecules form nanotubular



Scheme 1. Synthesis of 1,2-phenylenediboronic acid (**1**) and equilibrium between the acid and its semianhydride (**1-sanh**) in solution. [Reprinted with permission from K. Durka *et al.*, *Cryst. Growth Des.* 2013, 13, 4181. Copyright 2013 American Chemical Society.]

motifs, distinguishes this acid from its previously studied isomers. This is a very elegant example of HOF (hydrogen-bonded organic framework) crystal architecture based on small organic molecules. Figure 1 shows the projections of the unit cells illustrating the three crystal structures of *ortho*-phenylenediboronic acid in the notation used in the original publication. These are the trigonal form **1a** ($R\bar{3}$ space group) and two monoclinic forms – hydrate **1b** and the anhydrous form **1c** ($P2_1/n$ space group symmetry in both cases). In order to achieve the highest quality models of the obtained crystal structures, I conducted structural refinement applying the aspherical scattering factors. Using experience from my PhD studies, and the already

modelled pseudoatoms² of boron, oxygen and carbon for the boronic group (*i.e.* $\text{C-B}(\text{OH})_2$, the mentioned atoms are highlighted) present in the UBDB³ databank (University at Buffalo Data Bank), I performed TAAM⁴ (transferable aspherical atom model) refinements for the previously collected diffraction data, and determined crystal structures. Employing a more sophisticated electron-density distribution model, we managed to eliminate signals on residual electron density maps originating from bond formation, which are not taken into account by the IAM model. The final models obtained in this way are usually very similar to those determined on

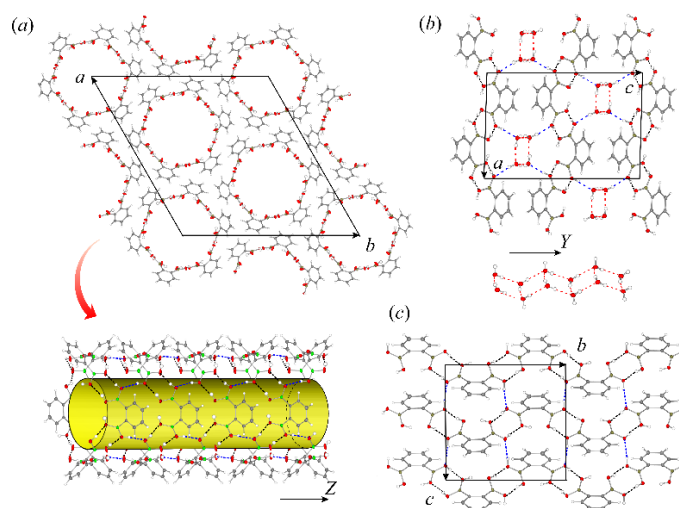


Figure 1. Packing diagrams showing the nanotubular architecture with 3-fold-axis symmetry in the **1a** ortho-phenylenediboronic acid structure (a), ordered water-molecule channels in the **1b** form (b) and molecular layers in the **1c** form (c). [Reprinted with permission from K. Durka *et al.*, *Cryst. Growth Des.* **2013**, *13*, 4181. Copyright 2013 American Chemical Society.]

the basis of the neutron diffraction data (I examined this aspect during my PhD for a series of uracil derivatives [P32], see also: [42]). While the anhydrous **1c** structure constituted a model case for application of the TAAM formalism, the other two systems were more problematic. The structure **1b**, in which two water molecules fall on one acid moiety, had to be refined taking into account the disorder of hydrogen atoms. The same applied for the structure **1a**, which however, despite the treatments performed, still did not fully reflect the experimental diffraction data. In this case, the acid molecules form channels of 3-fold axis symmetry ($\bar{3}$ inversion axis is present in the structure), inside which we observed signals not taken account of in the model. We estimated the channels' diameter to be about 8.8 Å, and established that they contain water molecules trapped during the crystallisation process. We performed the refinement of the structure framework composed exclusively of the acid molecules by using the SQUEEZE method [43]. However, to run periodic calculations in the *CRYSTAL* program [44-45], it was still necessary to propose the distribution of water molecules inside the 'nanotubes'. For this purpose, I came up with possible configurations of water molecules in one-to-one ratio

² In a certain simplification the electron density in ASU can be expressed as a sum of finite multipolar expansions localised at atomic positions [37]. Every such expansion is called a pseudoatom. In experimental charge-density studies the pseudoatoms consist of spherical atomic core and valence terms and the deformation part composed of spherical harmonics (*e.g.* in the Hansen-Coppens formalism [38]). In the procedure leading to the electron-density determination from X-ray diffraction data, the valence and deformation part populations are refined in addition to positional and thermal motion parameters. More details can be found in the book by P. Coppens [39].

³ Using experimentally- or theoretically-derived structure factors it is possible to refine the pseudoatom parameters for practically every molecule. Such pseudoatoms can be grouped dependent on their chemical environment yielding pseudoatom parameter data bases. Out of three such data bases – ELMAM [40], Invarions [41] and UBDB – during my PhD studies I was involved in the development and application of the last one [P27,P29,P32-P34,P36,P38].

⁴ In the TAAM approach the same parameters as in IAM (independent atom model) are refined, *i.e.* atomic positions and thermal motion parameters, but applying rigid aspherical form factors transferred from the pseudoatom data base.

(suggested by the thermogravimetric experiments – TGA), or in two-to-one ratio (maximum rational number of water molecules in the structural voids while maintaining the $R\bar{3}$ symmetry) when compared to **odba** molecules, and carried out optimisations of the structures constructed in such way (DFT(B3LYP)/6-31G** level of theory). The most advantageous energy results were obtained in the second case, *i.e.* for the model assuming two molecules of water per one acid molecule. The optimised structure of the polymer consisting of water molecules filling the channels resembled structural motifs occurring in crystals of hexagonal (ice I_h, $P6_3/mmc$ space group) or trigonal ice (ice II, $R\bar{3}$ space group), in particular the latter one (Figure 2). Considering the results of TGA experiments, we finally proposed the domain model of the structure **1a**. I also performed cohesive energy calculations for the remaining crystal forms, both for the TAAM-refined crystal structures and these after structure optimisation, both with, or without solvent. In the article [H1] we compared all structures and their energetic aspects. Interestingly, it appeared that the structure framework built exclusively of **odba** acid molecules is most energetically favourable for the **1a** system (energy trends derived for the TAAM-refined and optimised crystal structures are in agreement). Indeed, it is easier to grow crystals of the nanotubular form than the anhydrous form **1c**. At this point it should be noted, however, that other factors, such as entropy or kinetic effects, may also influence the crystallisation process. In contrast, in the **1b** structure, in which water molecules create strongest interactions with the **odba**, solvent contribution to the cohesion energy is most significant. This form crystallises as the only one, and only if at least two-fold excess of water over acid is provided. Interestingly, it is easier to remove water from this structure than from **1a**. The dehydration process is though associated with the simultaneous loss of sample's crystallinity.

[H2] **Dyes Pigm., 2017, 138, 267.** It turned out that *ortho*-phenylenediboronic acid differs from the *para* and *meta* isomers not only in the crystal structures formed by the pure compound, but also in reactivity with other chemical species. Inspired by the variety of the **odba** crystal forms, I became interested in the possibility of using it as a cocrystal component. Therefore, I made an attempt to obtain a cocrystal of **odba** with 8-hydroxyquinoline (**8-HQ**) – a model compound that could introduce the photoactive fragment into the crystal structure. When

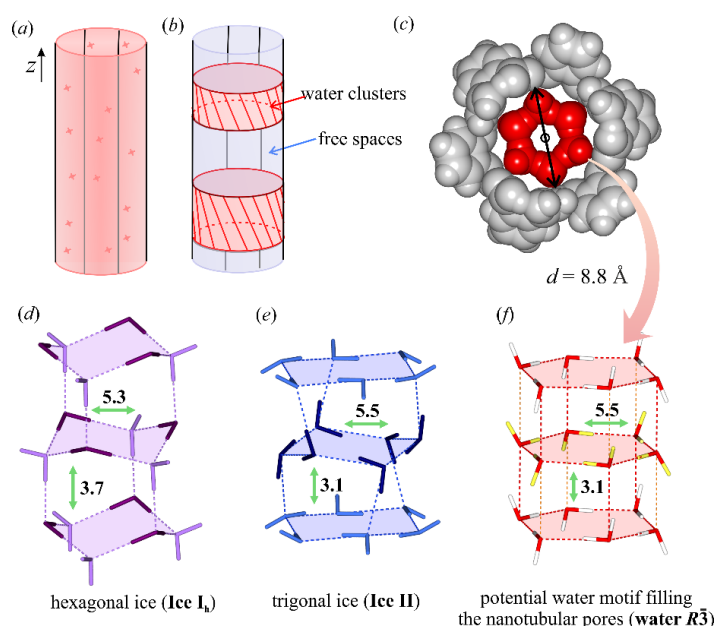
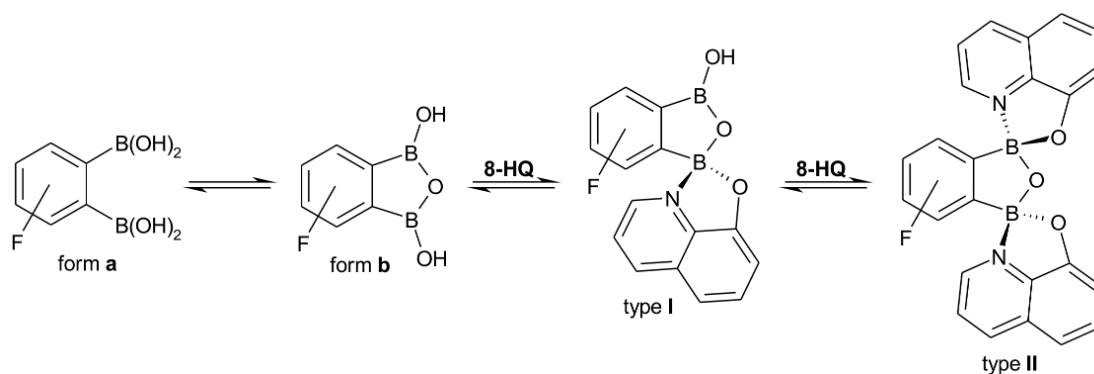


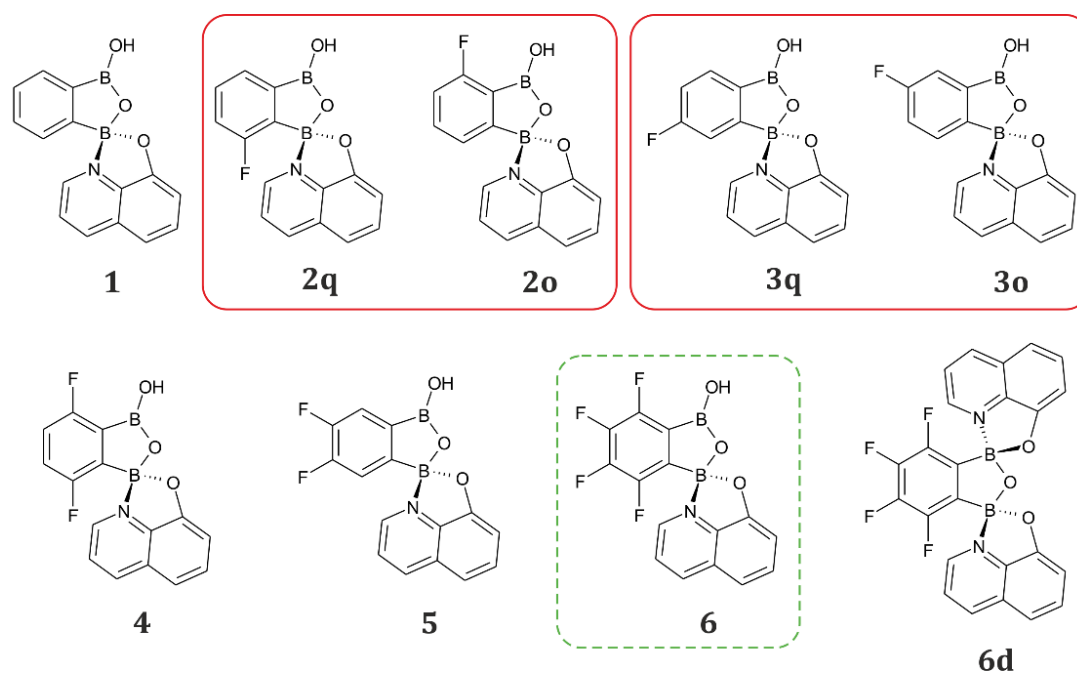
Figure 2. Schematic representation of two models for the association of water molecules inside the nanotubular channels: (a) random distribution and (b) domain structure. (c) The space-filling diagram viewed along the Z axis. Water-based polymeric motifs with 3-fold symmetry: (d) ice I_h ($P6_3/mmc$ group), (e) ice II ($R\bar{3}$), and (f) a potential water motif fitted to the **1a** boronic acid tube ($R\bar{3}$ symmetry). Different colours indicate symmetry-independent water molecules. [Reprinted with permission from K. Durka *et al.*, *Cryst. Growth Des.* **2013**, *13*, 4181. Copyright 2013 American Chemical Society.]

mixing the colourless solutions of both compounds in common organic solvents (acetone, acetonitrile, dichloromethane, tetrahydrofuran, or 1,4-dioxane), I observed a colour change to yellow-green, suggesting that these substances reacted with each other. Slow evaporation of solvent resulted in the formation of high-quality yellow-green crystals, which I subjected to X-ray diffraction experiments. It appeared that, indeed, *ortho*-phenylenediboronic acid had reacted with the 8-hydroxyquinoline. This was an interesting result, as no reactivity of boronic acids towards the **8-HQ**-type compounds has to date been noted. Thus, I obtained the first luminescent boronic 8-oxyquinolinato complex. In the discussed case, the close mutual location of the boronic groups in the aromatic ring, which were simultaneously involved in the reaction, proved to be of key importance. In solution **odba** occurs in equilibrium with its semianhydrate **[H1]** (Schemes 1 & 2). This semianhydrate, with two unsaturated acidic centres according to the Lewis theory, readily reacts with the (*N,O*)-donor compound, such as the applied **8-HQ** (Scheme 2). The simple synthesis of new photoactive complexes undoubtedly constitutes an advantage in the context of their application potential (it should be noted that the initial **odba** acid can also be relatively easily obtained). Furthermore, in view of the fact that *ortho*-phenylenediboronic acid may exist in the form of a semianhydrate it occurred to K. Durka that it should be possible to obtain its 8-oxyquinolinato complex in a mechanochemical manner. Indeed, this reasoning proved to be correct – grinding of **odba** with 8-hydroxyquinoline in the mortar leads to the formation of the complex with almost quantitative yield.



Scheme 2. Equilibria present in solutions of complexes of the studied **odba** derivatives with **8-HQ**.

In parallel to these studies, K. Durka and S. Luliński worked on the synthesis of fluorinated **odba** derivatives [46]. In the published article, they made some suggestions on the Lewis acidity scale of boron atoms in the obtained compounds. In view of that, I thought it would be interesting to examine the influence of the Lewis acidity of boron centres on the complexation reaction of **odba** derivatives with **8-HQ**. K. Durka and S. Luliński agreed to synthesise larger amounts of the fluorinated acids for the purpose of my research, complementing the series with two new *mono*-substituted *ortho*-phenylenediboronic acids. As a consequence, together with my team, we synthesised and crystallised a whole group of new complexes shown in Scheme 3. For each of these systems we managed to determine the crystal structure via X-ray diffraction methods. It appeared that in the case of *tetra*-fluorophenylenediboronic acid (**tetra-F-odba**) the molecule of the resulting compound **6d** contains two 8-oxyquinolinato fragments bound to each of the two boron atoms. This is undoubtedly associated with a very high Lewis acidity of the boron centres in this **odba** derivative, due to the induction effect of four fluorine atoms in the aromatic ring [46]. Titrations of 8-hydroxyquinoline solutions with an acid and simultaneous measurements of UV-Vis absorption spectra (UV – ultraviolet, Vis – visible) showed the equilibrium nature of acid transformations into complexes with one and two 8-oxyquinolinato



Scheme 3. Schematic representation of the studied complexes. Abbreviations for complexes **2** and **3** indicate the position of the fluorine atom (**q** – at the side of the oxyquinolinato ligand (**Q**), **o** – at the OH group side); abbreviation for complex **6d** indicates the double 8-oxyquinolinato substitution.

ligands. In the case of the model complex, a preference towards formation of a mono-complexed form is observed, while for **tetra-F-odba** the corresponding complex with two 8-oxyquinolinato ligands in the molecule is favoured.

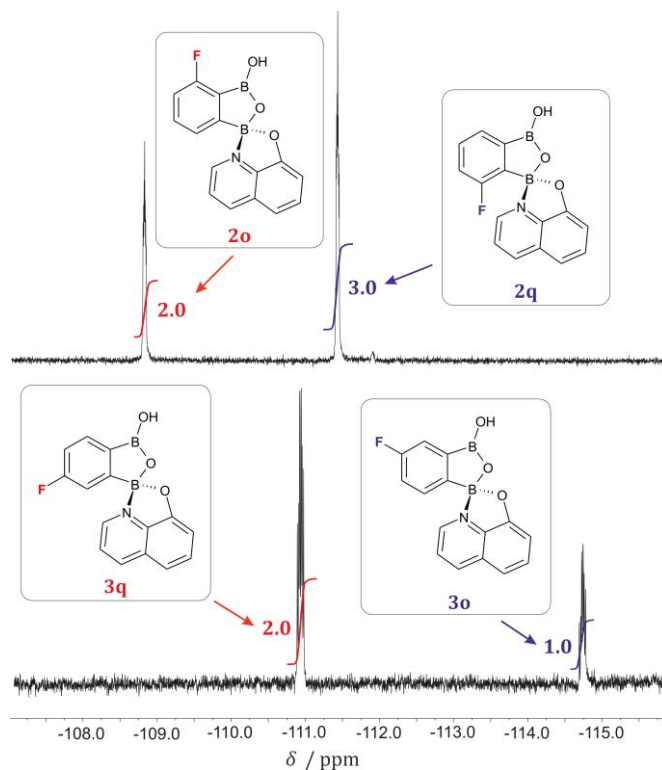


Figure 3. ^{19}F NMR spectra collected for **2q+2o** (upper spectrum) and **3q+3o** (bottom spectrum). The relative amounts of the **o** and **q** are additionally depicted.

Taking a closer look at Scheme 3, it can be noticed that systems **2** and **3** are formed by non-symmetric 3-fluoro- and 4-fluoro-1,2-phenylene-diboronic acids. The reaction of such acids with an equimolar amount of **8-HQ** can lead to isomeric complexes, referred to as the **q** and **o**-forms, in which the fluorine atom in the aromatic ring is located closer or further in respect to the 8-oxyquinolinato fragment. In solution these isomers exist in an equilibrium due to the possibility of reversible ligand dissociation. This process was monitored using ^{19}F NMR spectroscopy (Figure 3). In both cases we observed a notably larger amount of the **q** form. However, in the case of complex **2** the **q** isomer contains the more shielded fluorine atom, while for **3** the more deshielded one when compared to the fluorine atom in the

corresponding **o** form. The relative experimental chemical shifts were consistent with the computations I performed using the DFT(B3LYP, GIAO)/6-31++G(d,p) method including the polarisable medium as a solvent model (here chloroform). On the other hand, the relative chemical shifts of fluorine atoms registered in the ^{19}F NMR spectra, as well as the fact that the **q** form is preferred in both cases, can also be successfully explained via the analysis of substituent effects (*i.e.* mesomeric and induction effects associated with the influence of the electronegative fluorine atom in the aromatic ring on the boron atom; the greater Lewis acidity of the boron atom promotes the formation of the complex at this site). In addition, the **q** form was always a bit more energetically advantageous than **o** (by about 2.0–3.5 $\text{kJ}\cdot\text{mol}^{-1}$), which also supports the experimental observations. Interestingly, in the solid state the presence of both forms of complexes **2** and **3** leads to the disorder of the fluorine atoms, but the forms **q** and **o** occur in almost equal amounts (although always with a slight predominance of the **q** form).

Another interesting aspect of the studied compounds concerns their solid-state structures. It appeared that four complexes from the analysed series, *i.e.* **1**, **2**, **3** and **5**, form isomorphous crystal structures (Figure 4a). A dimer stabilised by hydrogen bonds between the B(O)OH moieties (Figure 4b) constitutes the main structural motif here. This dimer is also present in the structure of compound **4**, however, in the last case, due to the mutual location of two fluorine atoms in the molecule, the C–H \cdots F interactions are replaced by the F/H \cdots π contacts, which affected the resulting crystal packing. The structures formed by compounds **6** and **6d** are also very interesting. As I have already mentioned, and as shown in Scheme 2, the complexes in solution exist in a certain equilibrium. In the case of *tetra-F-odba* acid, this equilibrium is shifted towards form II. Nevertheless, crystallisation under air atmosphere leads to a mixture of crystals. Among them there are pure 8-hydroxyquinoline crystals, **6d**-containing crystals with **8-HQ** incorporated into their structure, and even cocrystals of forms I and II, *i.e.* **6** and **6d**. In such a cocrystal, dimers formed by molecules of **6** bound by the B(O)OH moieties are not formed, but mixed dimers of **6** and **6d** linked by one hydrogen bond between the free hydroxyl group of the **6** form and the oxygen atom binding the boron centres in the **6d** molecule, are present.

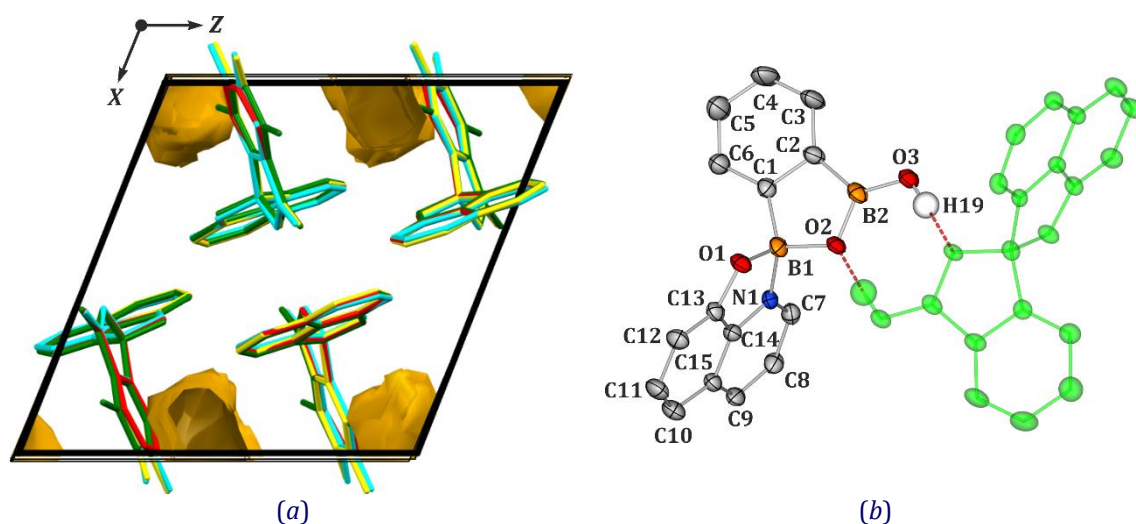


Figure 4. (a) Overlay of the unit cells of isostructural **1** (red), **2** (green), **3** (yellow) and **5** (cyan) crystal structures (solvent accessible surfaces are shown in yellowish colour). (b) Molecular structure of **1** and the main structural motif between symmetry-equivalent molecules present in crystals of most complexes (ellipsoids drawn at 50% probability level).

Spectroscopic properties of the new class of compounds constituted another important, and particularly interesting for me, element of the described research. All analysed systems are brightly fluorescent when excited by UV-light, both in solution and in the solid state. Solution samples exhibit emission with a maximum located around 525 nm, whereas in the case of the solid state we observed a shift of the emission maximum towards shorter wavelengths of about 25 nm (Figure 5). Such a result can be explained in a similar way as it was done by Liu *et al.* [47], *i.e.* through analysis of the manner in which molecules aggregate. For example, in the solid state the aromatic fragments of the luminescent systems are usually engaged mainly in $\pi\cdots\pi$ stacking interactions, which are considered to cause a red-shifted emission compared to that measured for diluted solution samples. In our case the situation is reversed, most likely due to the polarity of the complex molecules. If the crystallisation is driven majorly by polar interactions (in the crystal lattice there are, for example, hydrogen bonds), so that the molecules are located relatively further away one from another, it may result in strengthening of the observed luminescence and may also cause the emission blue-shift in respect to the spectrum of a diluted solution. I supported this hypothesis with the TDDFT (time-dependent density functional theory) computations conducted for selected dimeric motifs formed by the model system **1**, and the absorption spectra were indeed shifted towards higher energies when compared to the UV-Vis spectrum computed for an isolated molecule.

In the course of the research, we observed that the emission spectra for all compounds are similar, both in terms of energy range and shape. Furthermore, the luminescence decay times (about 9 ns) and quantum yields (about 15%) are very comparable for the studied complexes,

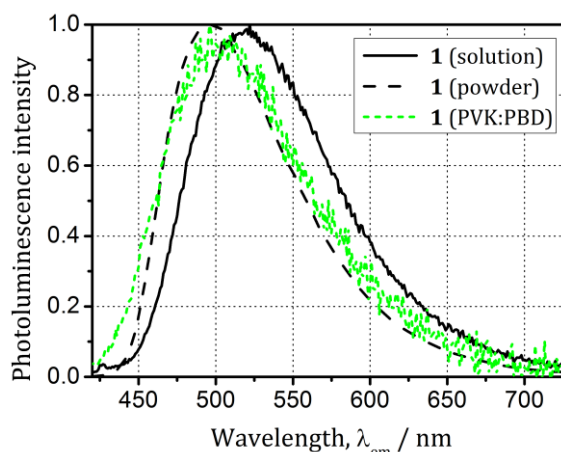


Figure 5. Normalised photoluminescence spectra for the compound **1** in acetone solution (black solid line), powder sample (black dashed line) and PVK:PBD matrix (green short-dashed line).

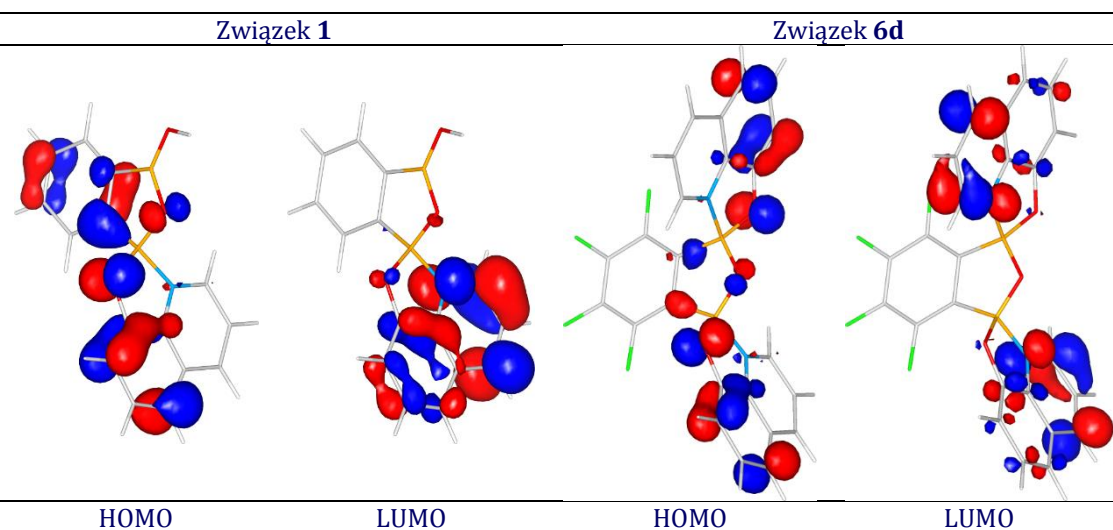


Figure 6. Selected molecular orbitals for compounds **1** and **6d** calculated at the DFT(PBE0)/6-31G** level of theory (isosurfaces: ± 0.05 a.u, blue – positive, red – negative).

even when relating the extreme cases – **1** and **6d**. Such behaviour could be explained by the singlet-singlet $\pi \rightarrow \pi^*$ excitation origin of the emission, in which the major contribution to the electronic transition is characterised by very similar energy values (*ca.* 3 eV) calculated between the highest occupied molecular orbital (HOMO) and the lowest unoccupied molecular orbital (LUMO), which is consistent with the cyclic voltammetry results obtained for derivatives **1** and **5**. The HOMO orbital is always centred on the oxadiborole fragment, whereas LUMO is localised majorly on the 8-oxyquinolinato ligand (Figure 6). Consequently, the aromatic ring substituents in the organoboronic fragment have little effect on the nature of the emission spectrum. On the other hand, it can be concluded that, as it is the case for the borinic systems [28], we should be able to control, to a certain extent, the emission colour via modifications of the (*N,O*)-donor fragment.

The design and evaluation of the OLED (organic light-emitting diode) efficiency based on the newly obtained complexes constituted the last important element of this study. Due to the fact that the construction of such a diode and the assessment of its parameters require specialised equipment and extensive experience, these studies were carried out by experts from the Lodz University of Technology – Ireneusz Głowacki and his PhD student Ewelina Witkowska – as a part of our cooperation. For that purpose, we have constructed OLEDs using two compounds, **1** and **6d**, as model examples. These compounds were placed in a polymer matrix made of poly(*N*-vinylcarbazole) (PVK) and 2-*tert*-butylphenyl-5-biphenyl-1,3,4-oxadiazole (PBD). It appeared that in both cases, the produced layers of the examined material exhibit electroluminescence, and the current-voltage characteristics of a respective diode has a typical shape (Figure 7) [48]. Comparing electroluminescence and photoluminescence, it can be concluded that the electroluminescence is red-shifted by about 20–30 nm for both compounds tested. The turn-on voltage at which the diode shows luminance 1 $\text{cd}\cdot\text{m}^{-2}$ equals approximately 7–9 V. Luminance greater than 400 $\text{cd}\cdot\text{m}^{-2}$ at 14 V and better current efficiency of the diode is observed for compound **1**. Such outcomes can be considered as rather good as far as other luminescent boron complexes are concerned [27] (it should be emphasised here that the diode was not optimised in terms of efficiency, as it is the case for many examples described in the literature). It also turns out that both compounds exhibit stable green emission, which is a desirable feature. This result is consistent with their relatively high thermal stability determined on the basis of differential scanning calorimetry (DSC) measurements.

[H3] Cryst. Growth Des., 2017, 17, 6836. Inspired by the multitude of isomorphous crystal structures formed by the compounds described in the previous work [H2], in the next article I devoted my attention to the aspects of crystal engineering of the new systems. For this purpose I made an attempt to obtain a series of crystals of the same compound containing molecules of various solvents in the structure. The crystallisation of a given chemical substance in the form of different solvatomorphs may be of great importance in the context of controlling the macroscopic properties of crystals. The model compound **1** constituted a natural candidate for such investigations (easy and efficient synthesis). At the beginning, I carefully inspected the

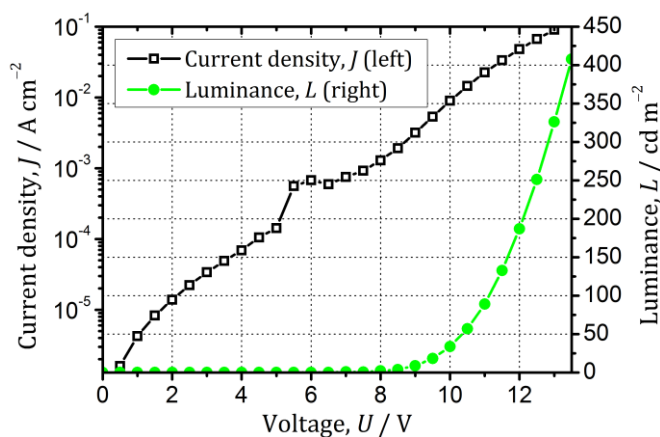


Figure 7. Current density (black squares) and luminance (green circles) vs. voltage for OLED based on compound **1**.

previously determined **1ace** structure (formed by the compound **1** when crystallised from acetone). In this case each molecule of the complex species comes with one half of an acetone molecule, which in combination with the observed crystal symmetry ($P2_1/c$ space group) enforces some solvent disorder (acetone is located at the centre of symmetry). Hence, I decided to examine whether it is possible to select of a solvent in a way to eliminate such

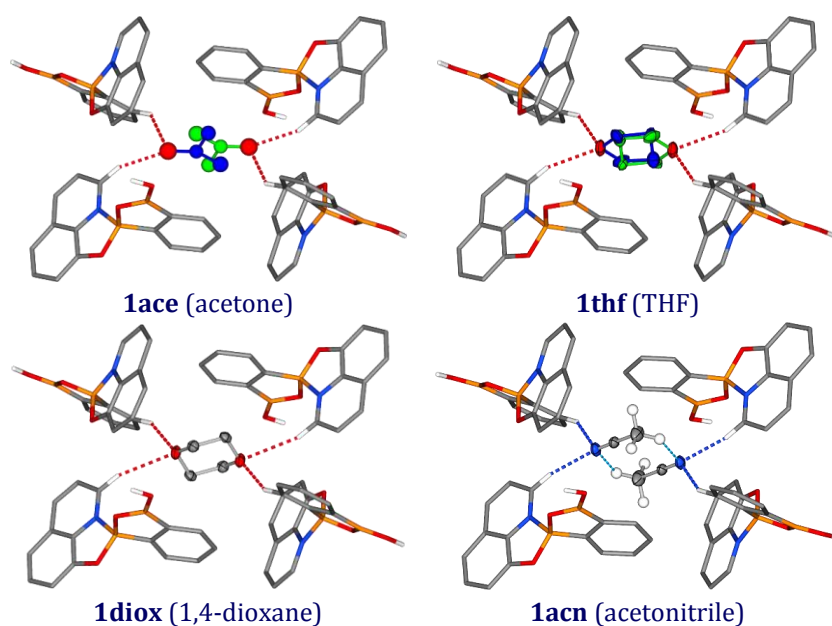


Figure 8. Solvent molecules and their nearest environment for isomorphous crystal structures of **1**. Disordered solvent molecules in **1ace** and **1thf** structures are coloured. [Reprinted with permission from K. N. Jarzemska *et al.*, *Cryst. Growth Des.* **2017**, *17*, 6836. Copyright 2017 American Chemical Society.]

disorder, and also to check how the nature of the solvent (molecule size, degree of polarity, *etc.*) used in the crystallisation process affects the crystal architecture. As compound **1** was soluble in typical organic solvents, we managed to obtain a series of crystals using acetonitrile, dichloromethane (DCM), tetrahydrofuran (THF), 1,4-dioxane, or methanol besides acetone (Figure 8). Thanks to X-ray diffraction measurements, we determined crystal structures of all types of grown crystals (in each case using the TAAM refinement). The results confirmed that in each case the solvent became in some way incorporated in the crystal structure. It turned out that the use of tetrahydrofuran (**1thf** structure), structurally comparable to acetone, induces situation resembling that encountered in **1ace**. In this case we observe an analogous disorder of the solvent species and very similar pattern of hydrogen bonds formed between the solvent and complex molecules. It is worth noting, however, that in both compared crystal structures the orientation of the lone electron pairs of the oxygen atom in the acetone and THF molecules are different, which I confirmed by appropriate deformation density maps. Via inspection of the structural cavity hosting the solvent species and the behaviour of the acetone and THF molecules, I could propose a solvent characterised by a suitable size and symmetry to optimally build into the complex **1** framework. Both conditions were rather well fulfilled by the 1,4-dioxane molecule, which is centrosymmetric in a chair conformation. Indeed, the use of this solvent resulted in the formation of high-quality crystals exhibiting the structure isomorphous to **1ace** and **1thf**, however, this time containing ordered molecules of 1,4-dioxane linking 4 complex molecules each. **1acn** grown from acetonitrile closed the isomorphous series. In this case, the cavity is occupied by two centre-of-symmetry-related solvent molecules that show solely rotational disorder of the methyl group. In the studied isomorphous crystal structures, the molecule of **1** is surrounded by 10 other complex species, which altogether form 6 independent dimers. The energetic analysis of intermolecular interactions confirmed that the most preferred structural motif is a centrosymmetric dimer stabilised by hydrogen bonds formed between the B(O)OH moieties. It also showed that although other intermolecular contacts, including C–H⋯O,

C–H $\cdots\pi$, or $\pi\cdots\pi$ interactions, are significantly weaker, when considered collectively they are very important in the context of the crystal lattice stability, as a whole. We also investigated the size of the cavity in all the crystals and the manner of the packing in which solvent species are incorporated into the structure. Additionally, we quantified the similarity between the studied crystal structures, including the previously measured isomorphous crystal structures of fluorine derivatives, using the *XPAC* program [49-50]. It appeared that **1ace** and **1thf** are most alike.

The use of dichloromethane, a solvent significantly sterically and physicochemically different from the ones already examined, led to the formation of the **1dcm** solvatomorph. Despite the same space group, ASU of **1dcm** consists of two molecules of the complex and two solvent moieties, among which, one is disordered. Nevertheless, in the **1dcm** crystal structure molecules of **1** create many structural motifs resembling those present in the analysed series of isomorphous systems. We have thoroughly examined the degree of this similarity, both in terms of geometry and energy. Furthermore, we compared the **1dcm** structure to the previously-determined crystal structures of the fluorinated derivatives of **1** which also contained DCM [**H2**]. Crystallisation of the **8-HQ** complex with 4-fluoro-1,2-phenylenediboronic acid from DCM yielded an isomorphous system to the **1ace–1diox** series. Such result can be explained by the fluorine atom location in the aromatic ring of the acid fragment, which enables formation of the advantageous C–F \cdots Cl interactions partially replacing the C–H \cdots Cl contacts. Otherwise, the resultant crystal architecture somewhat differs, as it is the case for **1dcm**, and for the crystal structure of the 3,6-difluoro-1,2-phenylenediboronic acid complex.

An interesting, and at the same time the most divergent result was obtained when crystallising the compound **1** from methanol. It occurred that **1** reacted with the solvent forming an ester **2**. Such an outcome shows that complex **1** can be functionalised using its free hydroxyl group at the 3-coordinated boron atom. This, in turn, constitutes its potential application advantage over borinic derivatives. In the used crystallisation conditions (a simple solvent evaporation method), the compound **2** is not entirely stable (the esterification is an equilibrium process), therefore both molecules **1** and **2** are present in the resulting **2meoh** crystal structure. Ester molecules constitute about 75% sites in the crystal structure. These species overlap in the unit cell with molecules of **1** (there is a disorder on the oxygen atom from the OH/OMe group). **2meoh** is also the only structure in which the classic dimer stabilised by hydrogen bonds is not present. The energy calculations, which I performed for three hypothetical crystal structures, *i.e.* for a structure containing solely the form **1**, for an analogous structure composed of **2**, and for a mixed one (the proportion of both forms was 50%), confirmed that interactions of the **2** \cdots **2** type are on average slightly more advantageous than the remaining kinds, which is reflected in the lowest cohesive energy calculated for the respective crystal.

In order to establish the relative stability of the studied crystal structures, I conducted cohesive energy periodic calculations for all other examined systems, as well as, commissioned the DSC measurements. Naturally, the results of both methods cannot be directly compared, however, together they provide a deeper insight into the thermodynamics of the analysed series. The cohesive energy values derived for the studied crystal structures are within expectations. In the group of the isomorphous structures, **1diox** and **1acn** are characterised by the most advantageous cohesive energy, while the least favourable one was obtained for **1ace**, which contains solvent species worst fit in the cavity. In turn, cohesive energy evaluated for **1dcm** is comparable to that obtained for **1thf**. Interestingly, the cohesive energy calculated for the framework structures, *i.e.* after removal of solvent molecules, is very similar in most of the cases, including **2meoh** and the fluorinated derivatives. The only exception from this rule is **1dcm**, in which the participation of DCM in the stabilization of the network proved to be most significant

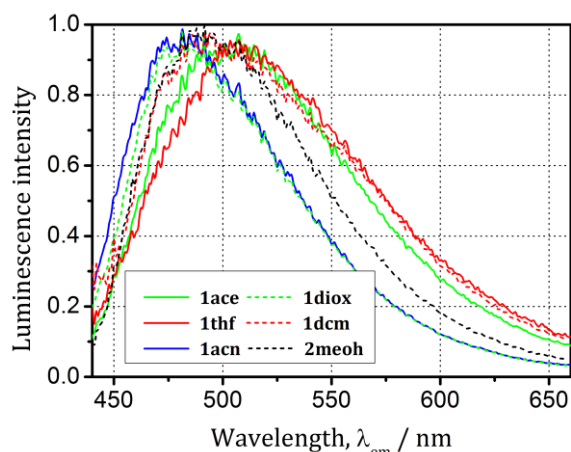


Figure 9. Single-crystal emission spectra for the studied solvatomorphs of **1** (including the **2meoh** structure) measured at room temperature. [Reprinted with permission from K. N. Jarzemska *et al.*, *Cryst. Growth Des.* **2017**, *17*, 6836. Copyright 2017 American Chemical Society.]

consequence, in solution the shift of the emission maximum was not observed and in each case it was located in the vicinity of 525 nm. For crystal samples, these differences became slightly larger and reached up to 30 nm (Figure 9), but the position and shape of the emission spectra were almost independent of temperature (studied temperature range: 90–300 K). On the other hand, the emission decay times oscillate around 15 ns, except for the shorter ones determined for the **1ace** and **1thf** crystals. The observed differences, however, diminish at low temperatures.

[H4] J. Phys. Chem. A, 2018, 122, 4508.

Based on the outcomes of the study described in the article [**H3**], it occurred to me that stable and high-quality crystals of the model complex **1** containing 1,4-dioxane as a solvent should be suitable for high-resolution X-ray diffraction experiments. This, in turn, would allow determination of the electron density distribution in the crystal of **1** in the ground state, which could to some extent be related to the observed spectroscopic properties. Consequently, together with K. Durka, we performed such an experiment ($(\sin \theta / \lambda)_{\max} = 1.2 \text{ \AA}^{-1}$) at 90 K. I processed the acquired data and modelled the charge density distribution using the Hansen-Coppens formalism [38], the analysis of which I conducted applying the QTAIM method⁵ (quantum theory of atoms in molecules) [51].

(the strongest complex...solvent interactions). Importantly, all systems can be considered relatively thermally stable with melting points oscillating around 200°C. The described observations were confirmed by results of crystallisations of **1** from mixtures of various solvents in ratios corresponding to their relative vapour pressure. Indeed, the more energetically stable form always crystallised best.

Finally, in order to better understand the spectroscopic properties of the studied complex **1**, I performed luminescence measurements for both solution and solid-state samples. The general conclusion coincides with that of the previous work [**H2**], as it appeared that solvent has rather little effect on emission properties. As a

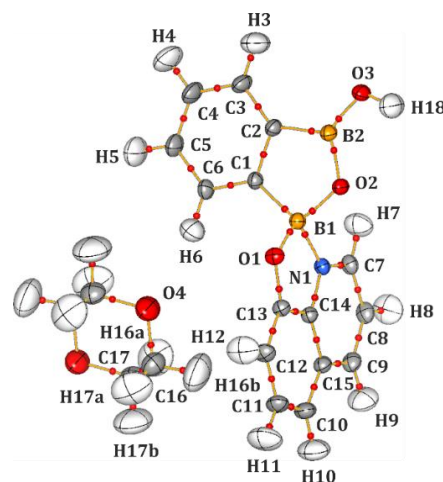


Figure 10. Molecular graph showing bond paths and bond critical points in **1diox** single crystal. Atom labelling and estimation of atomic thermal motion as ADPs is included (ellipsoids are drawn at the 70% probability level). [Reprinted with permission from K. N. Jarzemska *et al.*, *J. Phys. Chem. A* **2018**, *122*, 4508. Copyright 2018 American Chemical Society.]

⁵ The QTAIM approach concerns the analysis of the electron density distribution, $\rho(\mathbf{r})$ using well known multivariate calculus techniques. Between some atom pairs one can determine the so-called bond paths which correspond to the minimal gradient lines of $\rho(\mathbf{r})$. Places where $\nabla \rho(\mathbf{r}) = \mathbf{0}$ are called critical points, and based on the Hessian character, they can be classified as bond critical points, ring critical points, *etc.* The analysis of electron density Laplacian,

The obtained molecular graph and estimated atomic thermal vibrations are presented in Figure 10. In the context of atomic properties, the most interesting in the examined molecule are boron atoms, *i.e.* the 4-coordinated B1 and 3-coordinated B2. It appears that both atoms are described by very similar charges (+2.50 e for B1, +2.44 e for B2), as far as the method's accuracy is concerned [P26]. Such a result is somewhat intriguing because boron atoms with different coordination numbers are characterised by significantly different chemical and spectroscopic properties [4,56-57]. On the other hand, the 4-coordinated B1 centre is slightly more positive, which is consistent with the previous observations made on the basis of experimental data [56]. Both atoms, however, differ notably in terms of atomic volumes. It appeared that the volume of the 3-coordinated B2 atom is more than of 50% larger than that evaluated for B1. As expected, the acidic boron centres bare the most positive charge in the complex molecule, while the adjacent carbon atoms are characterised by the lowest charge values when compared to the remaining atoms of this element. All oxygen atoms and the nitrogen atom in the studied molecule form bonds with boron atoms and, thus, constitute the most negative sites of the complex. It also appeared that the obtained experimental values in general agreed well with the results of periodic calculations which I additionally performed (*CRYSTAL* and *TOPOND* programs [58-59], DFT(B3LYP)/pVTZ level of theory). The most pronounced discrepancies I noted here concerned the boron atoms, however, they may be explained by the shortcomings of both methods.

As a part of this study, I also carried out a thorough analysis of the bonds' nature in the molecule of complex **1**, in particular of the B–N connection. This interaction is interesting in the context of the earlier investigations of its lability, also carried out using the high-resolution X-ray diffraction method [56]. In the case of **1**, the determined value of the electron density at this bond critical point (BCP) amounts to $0.8 \text{ e}\cdot\text{\AA}^{-3}$, while its Laplacian equals $+10.3 \text{ e}\cdot\text{\AA}^{-5}$ (these results are in agreement with the theoretically-derived values, taking into account the method's precision). This suggests the partially ionic nature of the analysed bond. Interestingly, the analogous B–N bonding present in the previously examined azaester is characterised by negative Laplacian ($-4.36 \text{ e}\cdot\text{\AA}^{-5}$), which shows that such connection may also exhibit a dominant covalent character. Nevertheless, in the majority of literature reports, the sign of Laplacian is positive [60-62]. Such results confirm the lability of this bond (as previously shown in a certain area the Laplacian at the BCP of the B–N bond changes its sign [56]), which is of importance for understanding of the stability of these complexes in solution. This knowledge can be further used, for example, for the construction of dynamic 3-dimensional networks based on such interactions [63-65].

In the next step, I looked carefully at the intermolecular contacts. The performed QTAIM analysis confirmed and supplemented my previous conclusions based on geometrical parameters and calculated energy of weak interactions. In the course of the study I also noticed that the values of thermal motion parameters for the carbon and oxygen atoms of 1,4-dioxane are more pronounced than those estimated for atoms of **1**. This suggested that the structure of the crystal framework is composed of relatively strongly-associated complex molecules, while the solvent interacts weaker in its voids. This is reflected in the calculated or estimated interaction energies between **1** and dioxane and these stabilising the key complex dimers (*i.e.*

$\nabla^2\varrho(\mathbf{r})$, is also possible and may be very helpful. The analysis of the gradient of $\varrho(\mathbf{r})$ allows to partition the space via finding the surfaces where $\nabla\varrho(\mathbf{r}) \cdot \mathbf{n}(\mathbf{r}) = 0$. Inside such so-called atomic basins one can integrate, for example, the electron density yielding the atomic charge. Comprehensive analysis of all these parameters allows to understand the bonds' nature in a given molecule or crystal, evaluate the energetics of interactions, or even draw conclusions on the reactivity of the studied systems. More details about the method can be found in the available literature [51-55].

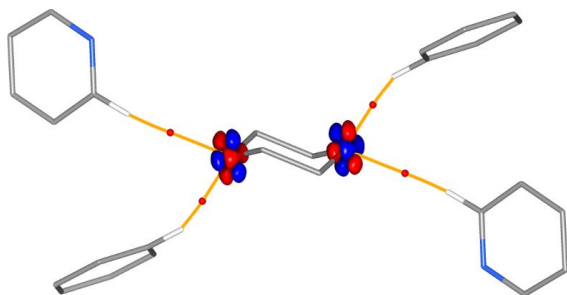


Figure 11. Difference of calculated anharmonic and harmonic dynamic electron densities in the vicinity of the dioxane molecule (both densities are computed with the same final geometry through the inverse FFT algorithm; isosurfaces: $\pm 0.25 \text{ e} \cdot \text{\AA}^{-3}$, blue - positive, red - negative). [Reprinted with permission from K. N. Jarzemska *et al.*, *J. Phys. Chem. A* **2018**, *122*, 4508. Copyright 2018 American Chemical Society.]

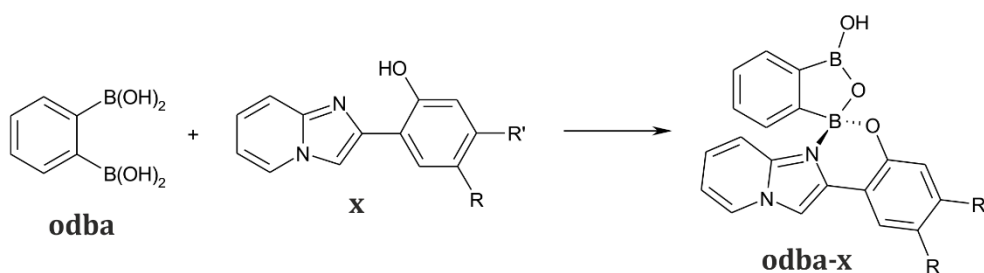
interpretation of the Gram-Charlier parameters is not fully clear, it is valuable to illustrate the modelled effects of anharmonic atomic thermal motion by generating a 3-dimensional difference map between dynamic anharmonic and harmonic charge density distributions (Figure 11). It seems that to date no one has analysed this type of differential maps, as only recently a relatively simple and fast method of calculating the dynamic electron-density-based on diffraction data has become available [74]. This map clearly shows the way in which the harmonic potential of oxygen atoms' vibrations is modified. Interestingly, these are the only atoms of the solvent species exhibiting noticeable thermal motion anharmonicity (this may be related to the nature of intermolecular interactions, but this aspect has not been sufficiently investigated, yet).

The last important element of this part of my project was an attempt to link the experimentally determined ground-state charge-density distribution with the spectroscopic properties of the analysed complex. This, however, was not a straightforward task. On the basis of the DFT(CAM-B3LYP)/6-31** computations it appeared that the HOMO \rightarrow LUMO and HOMO-1 \rightarrow LUMO transitions contribute most to the electronic excitation of the complex molecule from the ground state to the first singlet excited state ($S_0 \rightarrow S_1$). The shape of these molecular orbitals suggests that they are largely located on bonds, and therefore one should look at both atoms with the largest contribution to the molecular orbitals (within the LCAO-MO approximation - the linear combination of atomic orbitals-molecular orbitals), as well as the parameters of the respective interatomic bonds. In the case of the HOMO orbital, these are mainly C1-C2 and C1-B1 bonds from the organoboronic fragment, plus C10-C11, C12-C13 and C13-C14 from the 8-oxyquinolinato ligand. The former group shows rather low electron density values at BCPs, while the latter one shows the greatest values (it is worth noting here that the electron density value at BCP is most often correlated with the respective bond length [75-76]). The most significant atomic contributions to the HOMO orbital come from O2, C1 and C4 in the organoboronic part and O1, C10, C12, C13 and C14 in the 8-oxyquinolinato moiety. The oxygen atoms and the C1 carbon atom are strongly negative (as we know from the QTAIM analysis), the C13 and C14 atoms are positive, and the rest of the atoms exhibit charge values close to zero. In turn, the HOMO-1 orbital is, to a large extent, located on the acid fragment, in particular on the C1-C2 and C4-C5 bonds exhibiting quite low values of electron density at BCPs. However, all atoms that have the largest contribution to this orbital (O2, C1, C2, C4 and C5) are negatively charged. On the other hand, the LUMO orbital is located on the C7-C8, C11-C12, C13-C14,

1...1). In addition, due to stronger vibrations of solvent atoms (most significant for the O4 atom) the standard formalism in which atomic vibrations are described by means of harmonic approximation, is not sufficient. Characteristic alternating positive and negative values are observed in the residual electron density maps, [66-68],[P3, P18]. In order to account for these effects, I used a model of atomic vibrations extended by the 3rd order Gram-Charlier anharmonic parameters [69-71], which is available in the MOPRO suite [72-73]. Such a procedure indeed allowed a significant reduction of the mentioned residues. As the physical

C14–C15 bonds, most of which are characterised by relatively low electron density values at BCPs. In this case, atoms with the largest contribution to the molecular orbital bare positive charge, except for the N1 atom. Based on these observations it may be concluded that the HOMO–1 \rightarrow LUMO transition includes charge transfer from the acid fragment to the 8-oxyquinoline part, whereas HOMO \rightarrow LUMO has a mixed character with a predominant contribution of the $\pi \rightarrow \pi^*$ type on ligand. It should be stressed, that the latter transition, which most significantly contributes to the analysed electron excitation, determines the nature of the excited state. We managed, to some extent, to relate the experimentally evaluated charge density distribution to certain features of electronic excitations, which I consider to be quite significant. In addition, this work assured me that further modifications of this class of compounds should be carried out majorly within the (*N,O*)-donor ligand, as this fragment seems to be to a great extent responsible for the spectroscopic properties of the complex.

[H5] Acta Cryst. Sect. B, 2018, 74, 725. In the last article devoted to the boron compounds, I decided to examine the potential of **odba** to form complexes with a different group of (*N,O*)-donor compounds and to investigate the spectroscopic properties of the resulting systems. For this purpose I chose a series of luminescent 2-(2'-hydroxyphenyl)imidazo[1,2-*a*]pyridines synthesised by A. J. Stasyuk as part of his PhD [77]. Together with his supervisors, D. T. Gryko and M. K. Cyrański, they agreed to provide me with several compounds of this kind for the proposed research. It turned out that all four derivatives (Scheme 4) form photoactive complexes with the **odba** acid. We managed to successfully crystallise and determine crystal structures for three of them. In the course of this study, we also evaluated crystal structures for the derivatives **b** and **c**, as they have not been published yet. These structures are described in detail in the article, including the analysis of structural motifs and energy characteristics of intermolecular interactions. The **c** compound forms an isomorphic structure to that of the derivative with the methyl substituent at the R position previously described in the literature, which is also very similar to the structure of a derivative with the fluorine substituent (R = F). This is due to the high steric similarity of the methyl and bromine substituents. In the case of the derivative containing smaller and highly electronegative fluorine atom, the molecules are mutually slightly differently arranged, which facilitates the F...F interactions. The compound **b**, having a methoxy group at the R' position, crystallizes in a higher symmetry space group (*Pbca* vs. *P2₁/c*). Due to the presence of an additional oxygen atom in the molecule of this compound more hydrogen-bond-type interactions are present in the crystal. Nevertheless, in all structures we observe significant stacking interactions, whereas the cohesive energies of crystal structures formed by **b** and **c** differ only by about 1 kJ·mol⁻¹ in favour of **b**. It is also worth noting that in all four mentioned crystal structures of 2-(2'-hydroxyphenyl)imidazo[1,2-*a*]pyridines these compounds form an intramolecular hydrogen bond between the hydroxyl group and the



Scheme 4. Schematic representation of the reaction of **odba** with imidazo[1,2-*a*]pyridine derivatives (**x** = **a**: R = H, R' = H; **b**: R = H, R' = OMe; **c**: R = Br, R' = H; **d**: R = H, R' = Br). [Reproduced with permission of the International Union of Crystallography.]

nitrogen atom of the imidazole fragment. The possibility of this bond formation in solution, or its blocking by the solvent, is crucial for the luminescent properties exhibited by this group of systems, which can be classified as ES IPT (excited-state intramolecular proton transfer) compounds. This means that the proton transfer process in a molecule, which can be controlled *e.g.* by means of a suitably selected and located substituent in the phenyl ring, can significantly increase the Stokes shift of the emission spectrum, which in turn determines the colour of the observed luminescence.

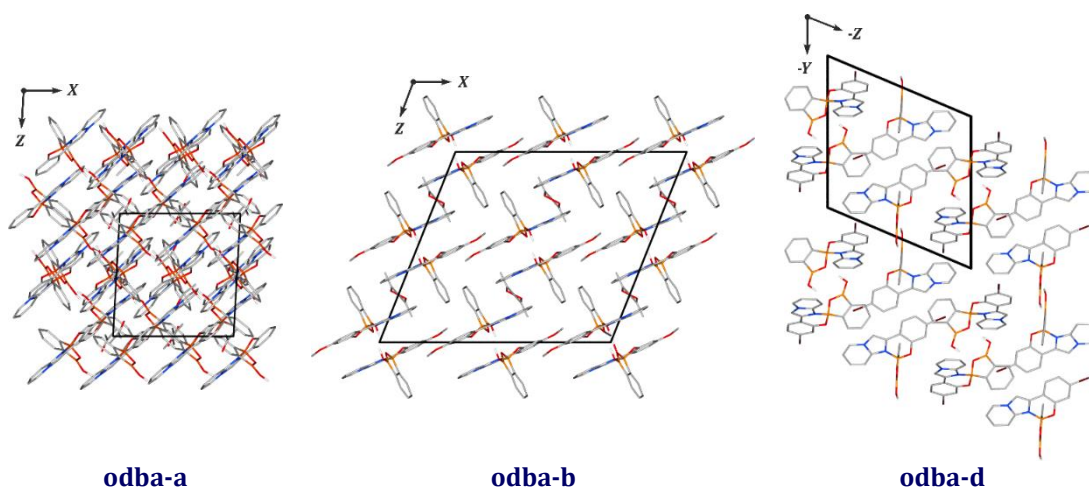


Figure 12. Crystal packing of the **odba** complexes with 2-(2'-hydroxyphenyl)imidazo[1,2-a]pyridines. [Reproduced with permission of the International Union of Crystallography.]

As far as the merits of this study are concerned, *i.e.* the complexes of 2-(2'-hydroxyphenyl)imidazo[1,2-a]pyridines with **odba**, I carried out the first reaction independently for the parent compound **a**, obtaining a model **odba-a** complex. In this case, I was also able to grow crystals suitable for further X-ray diffraction measurements and structure determination. The remaining X-ray measurements and all spectroscopic experiments were carried out under my supervision by S. E. Kutniewska (née Kutyla), my former undergraduate student, and currently my PhD student. The crystal structures were refined using the TAAM approach. It appeared that, unlike for 8-oxyquinolino complexes, obtaining good quality crystals of the synthesised compounds, *i.e.* **odba-a**, **odba-b** and **odba-d** was much more challenging (to the extent that in the case of the **odba-c** form we did not get crystals of sufficient quality), while the crystallisation process led to various crystal structures. Each complex crystallises in a different space group, and the structures differ also in the ASU content. The crystal packing of the three complexes is shown in Figure 12. **Odba-a** crystallises in the $P2_1$ space group with four complex molecules and four acetone species in ASU. **Odba-b** also forms a monoclinic solvate, but of higher symmetry ($C2/c$), whereas ASU in this case contains one complex moiety, and a half of an acetone molecule exhibiting disorder. In turn, the **odba-d** crystal structure is the only one that does not contain any solvent. In this case ASU consists of two molecules of the compound, while the crystal belongs to the $P\bar{1}$ space group. All three structures, however, share the main structural motif, *i.e.* a complex dimer stabilised via two hydrogen bonds between the B(O)OH fragment, analogous to that encountered in the previously-analysed crystals of **1** [**H2**]. In the currently discussed series such motifs are even slightly more energy-efficient. In all crystal structures significant stacking and C–H \cdots π -type interactions are also present. Despite the differences, the **odba-a** and **odba-b** crystal structures resemble **1ace** in terms of general features of crystal architecture. Considering the calculated

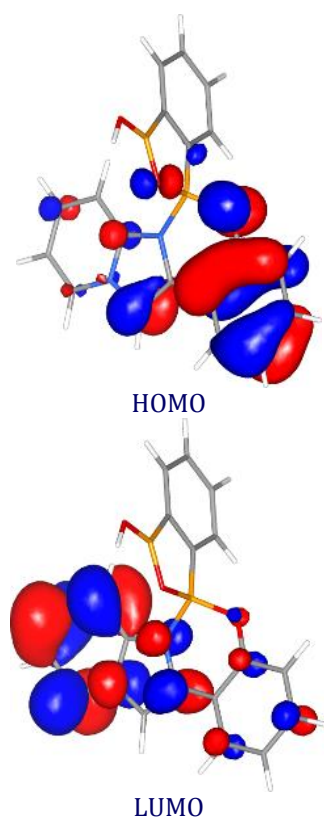


Figure 13. HOMO and LUMO orbitals for the **odba-a** compound calculated at the DFT(B3LYP)/6-311++G** level of theory (isosurfaces: ± 0.035 a.u.). [Reproduced with permission of the International Union of Crystallography.]

shown by pure 2-(2'-hydroxyphenyl)imidazo[1,2-*a*]pyridines, in which the ESIPT process is blocked, as shown by the emission spectra collected in acetone and toluene. The complexation of the compounds **a-d** in each case results in a reduction of the Stokes shift. As the complex formation reaction is an equilibrium process, the measured emission spectra include some signal coming from free luminescent **a-d** species. The observed emission bands' positions confirm the results reported by Stasyuk *et al.* [77]. Indeed, in an aprotic and non-polar solvent such as toluene, the ESIPT band is clearly seen (Figure 14). In a polar and aprotic solvent (acetone) ESIPT

cohesive energy, the structure of **odba-a** and its hypothetical non-solvent structure are most similar to the previously described isomorphous crystal structures of **1**. Additionally, in the case of **odba-a** the solvent contribution to the cohesive energy is greatest, which is in line with its largest content. In the **odba-b** crystal the energetic contribution of solvent is much smaller due to its disorder. However, this system is characterised by a more favourable cohesive energy calculated for the structure framework composed solely of complex molecules (after removal of acetone), when compared to **odba-a**. The most effective mutual arrangement of complex species is found in the crystal lattice of **odba-d**, as it allows for the saturation of intermolecular interactions without the use of a solvent.

The final stage of my project was to investigate and describe the spectroscopic properties of the newly-obtained complexes in solution, and characterise them by means of computational methods. In order to explore the nature of electronic excitations, I performed TDDFT calculations. These indicate that the HOMO and LUMO orbitals again contribute most to the lowest-energy electron transitions, but this time they are localised almost exclusively on the (*N,O*)-donor ligand (Figure 13). As a result, the charge transfer character of the excitation is significantly reduced when compared to that assumed for **odba-HQ** systems. The spectroscopic properties of the studied complexes are therefore very similar to those

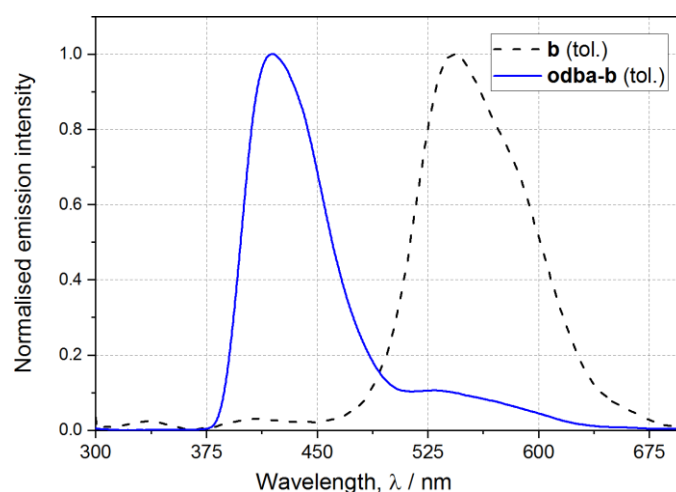


Figure 14. Example emission spectra for the **odba-b** compound measured in toluene (dashed line indicates spectra of the **b** compound before reaction with **odba**). [Reproduced with permission of the International Union of Crystallography.]

is, however, absent. Interestingly, after adding **odba** to the ligand acetone solution, the ESIPT band became visible. The substituents in the aromatic ring of the **a–d** compounds and their location undoubtedly influence the process of crystallisation, molecular packing in the crystal, as well as, spectroscopic properties, mainly because of differences in the complex–solvent interactions. Nevertheless, further research would be required to accurately explain the existing relationships.

4.3.3. Transition-metal complexes – structure, spectroscopy, photoelectrochemistry and time-resolved Laue photocrystallography

At the time of my studies on photoactive boron complexes, I also prepared a photocrystallographic research project and applied for funding within the “Mobility Plus” programme. For the destination of my postdoctoral stay I chose the University at Buffalo in the United States, namely the group of Philip Coppens, a pioneer in chemical crystallography and an outstanding specialist in charge density distribution studies and modern photocrystallography. This last area interested me most, especially the possibility of tracking structural changes, accompanying the light-induced charge transfer processes in molecular crystals, using the photocrystallographic techniques.

The term photocrystallography covers a set of combined spectroscopic and crystallographic techniques dedicated to studies of light-induced processes in crystals [78]. These methods are unique in a sense that they are practically the only ones that allow direct determination of a 3-dimensional structure of all types of metastable states beyond the ground-state crystal structure. A wide range of photocrystallographic methods includes studies of chemical reactions in crystals (*e.g.* dimerizations [79], *cis-trans* isomerizations [80], or radical reactions [81]), studies of long-lived excited states in transition-metal complexes (*e.g.* Fe, Ni or Ru) with NO, NO₂ or SO₂ ligands, showing (light-excited) configuration isomerism [82-86], or even the latest investigations of unstable transient forms occurring during catalytic cycles (*e.g.* elimination of chlorine molecules in dinuclear rhodium complexes [87]). New, greater possibilities concerning studies of light-induced structural changes have emerged along with the developments in the field of time-resolved synchrotron methods [83,88-89].⁶ Currently, it is feasible to capture in this way excited-state species lasting only fractions of nanoseconds (down to about 100 ps). Naturally, such measurements are very demanding, both experimentally and regarding data processing, the specificity of which depends on the character of the studied systems. The development of the time-resolved Laue method⁷ and its application for study of short-lived

⁶ Time-resolved synchrotron studies resemble the optical spectroscopy pump-probe methods. In this particular case the pump is the laser pulse, while the probe is the X-ray pulse (such experiments are then called laser-pump / X-ray probe). A synchrotron can produce X-ray pulses as short as 20–150 ps, dependent on its operation mode, maximal energy and other parameters. For the synchrotrons in the USA or in France where such experiments are feasible, the X-ray pulse duration is within the 80–100 ps range. Such single X-pulses are isolated from the synchrotron pulse train by means of various shutters and choppers, and then are electronically synchronised with the laser source [90-91].

⁷ In the Laue method the polychromatic radiation is used. This allows for more effective use of photons in the X-ray pulse [88-89], but it also leads to certain drawbacks during data collection and processing. In P. Coppens' group a series of methods to treat such data were developed and are described in details in the literature [92-100],[P6]. In particular, it is worth mentioning here the so-called RATIO method [101] in which the ratios of collected light-ON and light-OFF reflections are computed ($R = I^{ON}/I^{OFF} = |F^{ON}|^2/|F^{OFF}|^2$). This approach allows to eliminate the wavelength dependence. Such ratios are then used to estimate the structure factors for the excited structure (*i.e.* crystal structure in which both ground-state and excited-state molecules are present) based on the monochromatic

excited states in crystals of small molecules were among priorities of P. Coppens' group [102-105]. Experiments of this type usually give best results for systems containing heavier atoms (higher electron density turns into stronger X-ray diffraction signal) and undergoing significant structural deformations under irradiation. For these reasons, the above-described boron complexes, unfortunately, did not constitute simple research objects (the predicted structural changes, which I modelled using theoretical calculations, were rather subtle, while the complex molecules contained only relatively light atoms). Consequently, in order to master the method well, and also obtain interesting and useful results, I devoted my attention to photoactive transition-metal complexes. Such compounds often exhibit spectroscopic properties that could be effectively used to convert light energy into various forms of work in molecular systems, which indicates their wide application potential [1-2,106]. Multinuclear complexes of coinage metals, Cu, Ag or Au, which spectroscopic properties can be controlled *e.g.* by selection of organic ligands and/or by the number and type of metallic centres [107], are particularly interesting in this context. It is also worth noting that copper complexes can constitute a relatively cheap alternative to the currently-used expensive systems containing Rh, Ru, Pt or Ir. Experimental studies on spectroscopic properties and structural changes in such transition-metal complexes will provide information on the light-induced dynamics of molecules in crystals and the role of ligands and metallic centres (taking into account metal...metal interactions) in the context of macroscopic properties of such materials. In the longer perspective, these studies can contribute to the conscious design of functional materials, and may even lead to new and currently unexpected applications of such systems in optoelectronics and other fields.

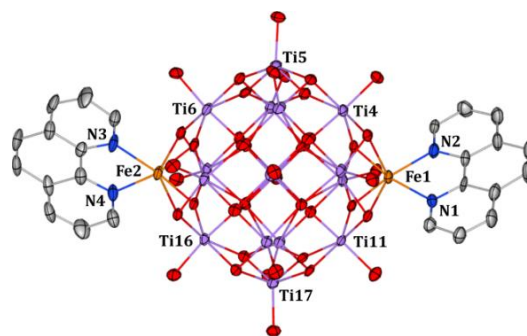


Figure 15. Molecular structure of the $\text{Ti}_{17}\text{O}_{28}(\text{O}^i\text{Pr})_{16}\text{Fe}_2(\text{phen})_2$ nanocluster (^iPr groups are omitted; 50% probability ellipsoids).

[H6] Phys. Chem. Chem. Phys., 2014, 16, 15792. I worked with P. Coppens in the years of 2013–2014. When I joined the group, Professor and his co-workers had already, for some time, been intensively investigating oxotitanate clusters [108-114], which are model systems for the analysis of charge transfer processes occurring in solar cells. Oxotitanate clusters imitate to a large extent the surface of titanium dioxide (TiO_2) used in such devices, in which the electron transfer takes place, and, importantly, they are characterised by a well-defined structure (these complexes are usually relatively easy to crystallise, so their structure can be determined via the X-ray diffraction technique). Furthermore, their spectroscopic properties can be modified using various transition metals as dopants. During my postdoctoral stay in Buffalo, naturally, I first became involved in photocrystallographic studies of titanium clusters, these being among the priorities of my “Mobility Plus” project.

data collected for the ground-state structure (*i.e.* composed solely of ground-state molecules) ($|F_{\text{est}}^{\text{ON}}| = \sqrt{R} \cdot |F_{\text{obs}}^{\text{mono,OFF}}|$).

Our literature studies resulted in finding, among others, an interesting paper devoted to photoelectrochemical investigations of two systems containing transition metals – cobalt and cadmium at +II oxidation state – incorporated into the core of the oxotitanate cluster of a general formula $\text{Ti}_{17}\text{O}_{28}(\text{O}^i\text{Pr})_{16}\text{M}_2(\text{phen})_2$ ($\text{M} = \text{Co}, \text{Cd}$; phen = 1,10-phenanthroline; ^iPr = isopropyl) [115]. The authors irradiated thin layers of these complexes with a xenon arc lamp and for the cobalt-containing sample they were able to observe some photocurrent described as cathodic. The experiment, however, was not well documented. In addition, the composition of the studied layer was questionable because this moisture-sensitive sample was prepared under air atmosphere, and an aqueous sodium sulphate solution was used as the electrolyte (measured Raman spectrum was also significantly different from that obtained for the pure compound). The authors did not examine the relationship between the photocurrent intensity and the excitation light wavelength.

For the purpose of a thorough investigation of the light-induced charge transfer process in this type of clusters, we obtained several analogues of the above systems, of which the most interesting was the iron(II) complex – $\text{Ti}_{17}\text{O}_{28}(\text{O}^i\text{Pr})_{16}\text{Fe}_2(\text{phen})_2$. I managed to determine the crystal structure of this compound, which is shown in Figure 15 (I omitted the alkoxy ligands bound to the core of the molecule). The analysis of the geometry of the molecule indicates that this cluster constitutes a modification of the previously-known system containing 17 titanium atoms ($\text{Ti}_{17}\text{O}_{24}(\text{O}^i\text{Pr})_{20}$) [108,116], and that the iron atom exhibits the high-spin electron configuration.

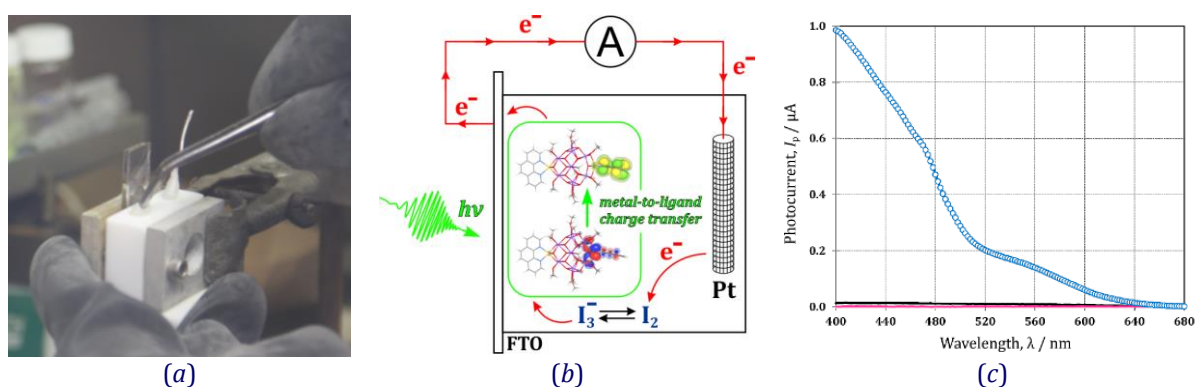


Figure 16. (a) Preparation of a photoelectrochemical cell inside a glovebox. (b) Scheme of the photoelectrochemical cell. (c) Photocurrent measured with the $\text{Ti}_{17}\text{O}_{28}(\text{O}^i\text{Pr})_{16}\text{Fe}_2(\text{phen})_2$ nanocluster films on FTO-covered quartz-glass plate (black and pink lines represent respectively the results of reference experiments conducted with a $\text{Ti}_{17}\text{O}_{24}(\text{O}^i\text{Pr})_{20}$ -complex-covered FTO electrode and a plain FTO slide as working electrode).

As part of this research, I also designed a photovoltaic cell based on the synthesised cluster, which I could use to generate and measure a potential photocurrent. For this purpose, I inserted a solution of iodine and potassium iodide (a redox couple) in acetonitrile into the available Teflon chamber, followed by a platinum electrode which I placed between two quartz plates, one of which had the inside surface coated with fluorine-doped tin oxide (FTO) with a thin layer of fine crystalline oxotitanate sample deposited by solvent evaporation. I prepared the necessary solutions and the entire photovoltaic cell in a glove box (Figure 16a). Such constructed photovoltaic cell was then placed in a setup for measurement of the photocurrent generated during irradiation (xenon arc lamp) of the electrode covered with the sample layer. The scheme illustrating the experiment is shown in Figure 16b. An exemplary photocurrent measured in this way is presented in Figure 16c. As can be seen, an anodic photocurrent occurred in the

wavelength range of *ca.* 400–640 nm. The recorded photocurrent is naturally significantly weaker than that achieved in many solar cells optimised for efficiency [117]. Nevertheless, the obtained results are fully reproducible, while the photocurrent intensity correlates with the thickness of the sample layer (thicker sample layers hamper the charge flow). We attributed the low efficiency of the examined process, among others, to the presence of alkoxy groups on the surface of the cluster core which limit the contact of the oxotitanate species with the FTO layer, thus

impeding the efficient charge transfer. Importantly, the lack of metal doping in the molecule, such as in the parent $\text{Ti}_{17}\text{O}_{24}(\text{O}^i\text{Pr})_{20}$ cluster which I examined in the same way, prevents the cell from working in the visible-light region, and consequently no photocurrent was observed.

In order to rationalise the results of photoelectrochemical measurements and combine them with the determined structure of the compound, I carried out theoretical calculations. Analysis of the density of states evaluated at the DFT(PBE0)/LANL2DZ level of theory indicated that two occupied iron β -orbitals are located inside the ‘energy gap’, which is not observed for the parent $\text{Ti}_{17}\text{O}_{24}(\text{O}^i\text{Pr})_{20}$ system. Such a distribution of molecular orbitals of the Fe cluster suggests reduction of energy portion needed to effectively excite the electron in this case. Therefore we expected the red shift of the absorption edge of the iron-doped sample as compared to the unmodified cluster. The TDDFT calculations conducted for the isolated complex molecule confirmed these assumptions. Moreover, the theoretical UV-Vis absorption spectrum agreed quite well with the experimental one, and reflected the spectral range of the measured photocurrent. We can distinguish here two types of low-energy excitations involving d electrons from the iron atom β orbitals (Figure 17). The charge is transferred from the Fe atom either to the phenanthroline ligand orbitals (MLCT, metal-to-ligand charge transfer) or to the oxotitanate core (MCCT, metal-to-core charge transfer). The exposed location of the phenanthroline fragment towards the outside of the core surrounded with the alkoxy ligands suggests that the MLCT transition is crucial for the operation of the studied photovoltaic cell (we observe the anodic current, *i.e.* the transfer of electrons from the clusters to the FTO).

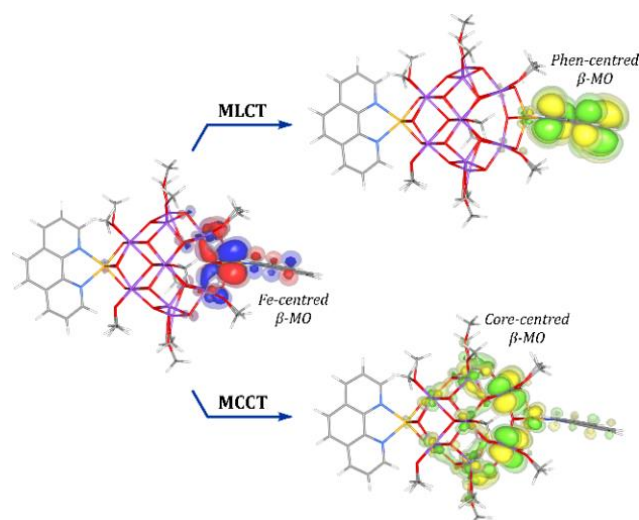
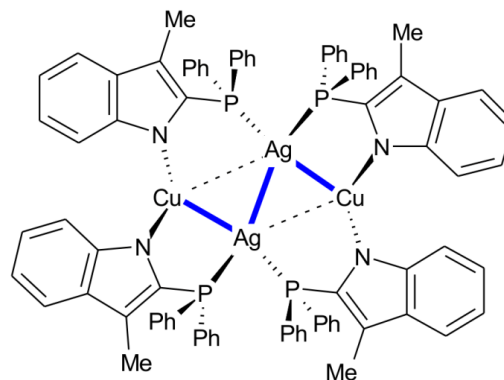


Figure 17. Visualisation of MLCT (top) and MCCT (bottom) transitions using molecular orbitals (solid isosurfaces: ± 0.02 a.u., semi-transparent: ± 0.01 a.u.).

It should be emphasised here that the presented work is one of, if not the first one, in which the crystallographic analysis was combined with photoelectrochemical studies for fully structurally defined photoactive titanium clusters. Although, regrettably, we have not been able to photocrystallographically observe the light-induced structural changes in the crystal of this compound, the obtained outcomes were interesting and useful. My experience regarding photoelectrochemical experiments and calculations of electronic transitions resulted in several subsequent projects [P10,P13,P17]. It is worth mentioning that the results of my photocurrent measurements (the direction of current flow in the cell) made as part of an important work on this subject [P17] confirmed the assumptions about the nature of the charge transfer process based on sophisticated theoretical analysis.

[H7] *Inorg. Chem.*, 2014, 53, 10594. Due to the difficulties associated with photocrystallographic observation of structural changes accompanying the charge transfer in oxotitanate clusters, I started studying literature in search for other interesting and important photoactive complexes. Inspired by P. Coppens' previous studies regarding metal...metal interactions [105,118-120], I decided that first a system containing at least two transition-metal atoms from the 3rd or higher period should be found which excited by UV-light, would show significant Stokes shift of emission. On the basis of the literature search performed by PhD student, J. D. Sokolow, we selected a promising complex, $\text{Ag}_2\text{Cu}_2\text{L}_4$ (L = 2-diphenylphosphino-3-methylindole) (Scheme 5), in which two silver(I) and two copper(I) atoms constituted the core of the molecule surrounded by organic ligands [121]. The synthesis and crystallisation of this system was carried out by J. D. Sokolow and Y. Chen, while its crystal structure was determined jointly by me and E. Trzop. Thanks to the



Scheme 5. Schematic representation of the studied $\text{Ag}_2\text{Cu}_2\text{L}_4$ complex (L = 2-diphenylphosphino-3-methylindole; Ag–Ag and two shorter Ag–Cu interactions are shown in bold). [Reprinted with permission from K. N. Jarzemska *et al.*, *Inorg. Chem.* 2014, 53, 10594. Copyright 2014 American Chemical Society.]

modification of the synthesis protocol and replacing chloroform with dichloromethane, we were able to obtain a crystal structure with no solvent content (the presence of a solvent is not desirable, since it can potentially cause faster crystal degradation under laser light irradiation). I recorded absorption and emission spectra for such obtained single crystals and measured the luminescence decay. The crystals exhibit orange-red emission (with the emission maximum at 650 nm). The determined excited state lifetime of about 1 μs suggested the phosphorescence of a triplet state origin. As the Stokes shift was significant, we could expect notable structural changes occurring under UV irradiation. In view of the above, this compound proved to be an excellent candidate for further research using the time-resolved Laue method, which we later performed on the 14-ID-B BioCARS beamline [90] of the Advanced Photon Source (APS) synchrotron, located at the Argonne National Laboratory near Chicago, in the United States. We prepared and conducted such experiments, and then processed the collected data (we used the RATIO method proposed earlier by P. Coppens *et al.* [101]), out of which the four best quality data sets were selected for further analysis. Figure 18a shows the resulting 3-dimensional

photodifference map,⁸ in which the blue peaks (positive difference electron density) indicate the approximate directions of the corresponding atoms' shifts about 100 ps after the laser pulse hit the crystal. As can be seen the largest signals are observed near the silver atoms, whereas some weaker and asymmetric ones next to the copper centres. Using the program named *LASER* [122], which among others enables quantitative analysis of changes in the molecule's geometry due to the excitation, and estimation of the excited-state population, we were able to refine the excited-state structure based on the measured synchrotron data and the reference monochromatic data of the studied system. After jointly establishing the best strategy, I carried out the final refinement, the result of which is shown in Figure 18b. In the studied case, the excited state population amounted to approximately 1%. This result was in line with my expectations, as it constituted the superposition of the relatively low power of the pumping laser selected to excite compound molecules, but also to minimise the crystal decay upon irradiation, and the moderate emission quantum yield [121]. The determined excited-state structure is in accordance with the premises derived

from the photodifference map. The most significant molecular geometry changes are noted for the Ag1...Cu2 and Ag1...Ag2 contacts (they shorten by 0.59(3) Å and 0.38(3) Å, respectively), which is associated with significant shifts of silver and Cu2 atoms. The shortening of the Ag-Ag distance down to

2.66(3) Å is particularly interesting, as this bond length is comparable to that of the shortest and strongest bonds formed between silver atoms ever described in the literature [123-124].

In order to explore the nature of electronic transitions in the studied complex, I performed TDDFT computations (DFT(PBE0)/LANL2DZ level of theory) for the isolated molecule. It appeared that excitations with the lowest energy are associated with electron transitions from the HOMO, HOMO-1, HOMO-2 and HOMO-3 orbitals, localised on the skatole ligands, to LUMO centred between silver atoms (Figure 19). Therefore, it can be concluded that the studied electronic transition is of the LMCT (ligand-to-metal charge transfer) type, and leads to the

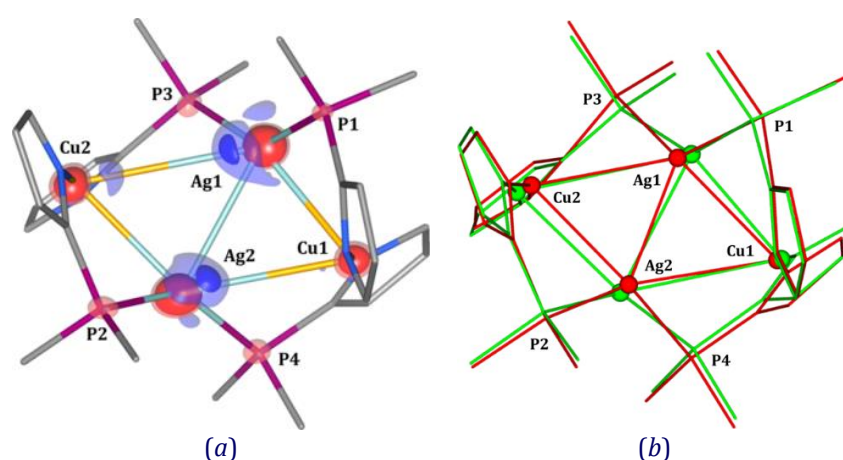


Figure 18. (a) Photodifference map showing atomic shifts upon excitation (solid isosurfaces: $\pm 0.55 \text{ e}\cdot\text{\AA}^{-3}$, semi-transparent: $\pm 0.35 \text{ e}\cdot\text{\AA}^{-3}$). (b) Refined excited-state structure related to that of the ground-state (green colour – ground state, red – excited state). Ligand fragments were omitted for clarity. [Reprinted with permission from K. N. Jarzemska *et al.*, *Inorg. Chem.* **2014**, *53*, 10594. Copyright 2014 American Chemical Society.]

⁸ The (Fourier) photodifference map indicates the electron density changes (*e.g.* atom shifts or temperature parameters' changes) under the light-induced excitation. To generate such maps both the reference ground-state structure ($F_{\text{obs}}^{\text{OFF}}$) and excited structure ($F_{\text{obs}}^{\text{ON}}$) structure factors are needed. For example:

$$\Delta\rho_{\text{pdiff}} = V^{-1} \sum_{\mathbf{h}} (|F_{\text{obs}}^{\text{ON}}(\mathbf{h})| - |F_{\text{obs}}^{\text{OFF}}(\mathbf{h})|) e^{i\varphi_{\text{calc}}^{\text{OFF}}(\mathbf{h})} e^{-2\pi i \mathbf{h} \cdot \mathbf{r}}$$

In the case of the Laue method the structure factors of the excited structure are estimated based on the measured intensity ratios (the RATIO method) and the reference monochromatic structure factors for the ground-state structure (*i.e.* $|F_{\text{obs}}^{\text{ON}}| \approx |F_{\text{est}}^{\text{ON}}| = \sqrt{R} \cdot |F_{\text{obs}}^{\text{mono,OFF}}|$).

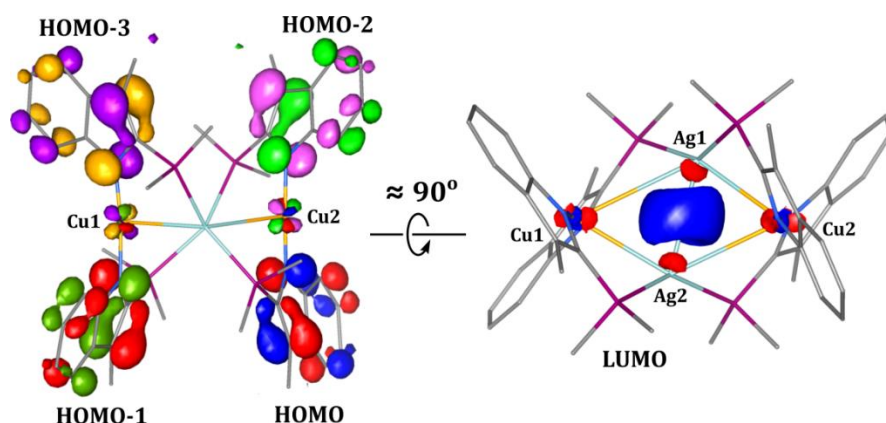


Figure 19. Composite picture of the molecular orbitals with the most significant contribution to the LMCT transition (level of theory: DFT(PBE0)/LANL2DZ). Isosurfaces: ± 0.06 a.u. Left panel – view along Ag–Ag bond. Ligand fragments were omitted for clarity. [Reprinted with permission from K. N. Jarzemska *et al.*, *Inorg. Chem.* **2014**, *53*, 10594. Copyright 2014 American Chemical Society.]

strengthening of the Ag–Ag interaction. The atomic charges calculated for both the ground- and excited-state molecules clearly show that the copper atoms change their charge only slightly during the excitation, whereas the electron density moves majorly from the skatole fragments to silver atoms and, to a little

extent, also to the bound phosphine ligands. As a result of this process silver centres become nearly neutral. This means that the charge redistribution in the molecule leads from formal silver(I) in the ground state to silver(0) in the excited state (“Ag^I → Ag⁰”), which also supports the Ag–Ag bond shortening.

An interesting aspect of my research also concerned the substantially asymmetric behaviour of the corresponding fragments of the complex molecule during the excitation, especially apparent in the case of metallic centres. The optimised isolated molecule of the compound is characterised by the ‘zig-zag’ pattern formed by metallophilic interactions in the metal core (Scheme 5), while the copper and silver atoms constitute the corners of the parallelogram. In the case of a crystal, complex molecules are deformed due to the crystal packing and intermolecular interactions. To determine the influence of the molecular environment in the crystal on the geometry of the complex species, both in the singlet ground state (GS) and in the first excited state (ES), I carried out two types of calculations. I optimised the geometry of the isolated molecule in GS and ES electronic states using the *GAUSSIAN* program [125], but also, applying the QM/MM (quantum mechanics / molecular mechanics) method, I optimised the molecule (in both electronic states) encapsulated in a cluster of molecules (*GAUSSIAN* input files were prepared using the *CLUSTERGEN* program [P28]) simulating the crystalline environment (Figure 20). This approach, despite its limitations, has so far performed very well in the context of estimating structural changes occurring in metal complexes upon light excitation [98,103,105,126]. It turned out that in our case, the agreement between experimental data and the QM/MM results was very good. Such modelling nearly perfectly

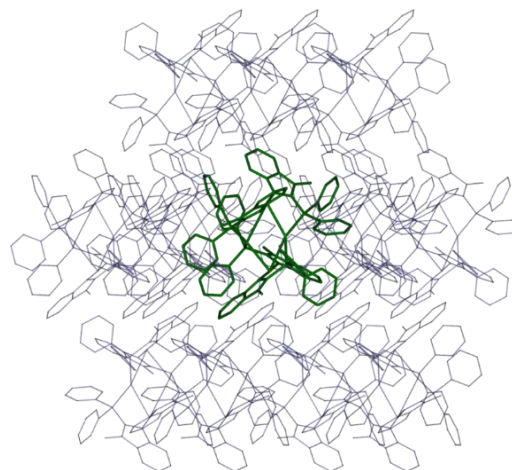


Figure 20. Molecule shell used in the QM/MM calculations (green – central molecule, grey – shell of 13 molecules within a radius of 10 Å). [Reprinted with permission from K. N. Jarzemska *et al.*, *Inorg. Chem.* **2014**, *53*, 10594. Copyright 2014 American Chemical Society.]

reflected the way in which molecules are deformed in the crystal, and reflected the trends of the experimental light-induced geometric changes. For instance, in the case of the Ag–Ag bonds a 0.345 Å reduction is predicted theoretically, while the experimental value is 0.38(3) Å. Similarly, the Ag1···Cu2 contact according to theory should be reduced by 0.622 Å, and the measured value equals to 0.59(3) Å. Moreover, even minor changes, for example of 0.06(3) Å, as in the case of the Ag1–Cu1 bond elongation, are well reproduced by the QM/MM method (extension by 0.086 Å). In general, the nature of electron excitation in this molecule induces contraction of the core and its deformation from ‘zig-zag’ (two longer Ag···Cu contacts, two shorter ones) in the ground state, to a rhombic-like shape (longer Ag···Cu shortens the most). The most pronounced discrepancies occur between the copper atoms’ shifts (0.09(2) Å and 0.33(3) Å for Cu1 and Cu2 atoms, respectively, calculated values: 0.10 Å and 0.26 Å), due to the fact that in the crystal, the molecules interact one with another either through ligands attached to the Cu1 atom in each of them, or both through the Cu2-related fragments. It is worth mentioning that the optimisation of the isolated molecule in the GS and ES states, as a result of neglecting of intermolecular interactions in the crystal lattice, leads not only to the higher symmetry of the molecule in both cases, but also to strongly overestimated structural changes. All these observations show how important it is to take into account the environment in which the process under study takes place. Comparability of the QM/MM and Laue method results also indicates that these approaches are very well justified.

Summing up the results presented above, the success of my work was undoubtedly the experimental determination of the structure for one of the shortest-living light-induced excited states studied to date by photocrystallographic methods, while achieving results highly consistent with theoretical predictions. I consider this study as one of my most important scientific achievements. It combines my experience in computational chemistry (for isolated and solid-state-embedded molecules), electron density distribution analysis (*e.g.* QTAIM method) with modern photocrystallographic methods, which are currently the core of my scientific activity. Thanks to this research and the acquired skills, I continued to work with P. Coppens for a period of time after completing the postdoctoral internship [P6,P10,P12,P13].

[H8] Inorg. Chem., 2018, 57, 8509. The deformation of the metal core upon electron excitation in the model luminescent copper(I) and silver(I) complex in the solid state described in the paper [H7] inspired me to verify whether similar structural distortions can be observed in the ground state by applying hydrostatic pressure to the crystal of the this compound. At the same time, a number of questions arised, including the impact of the molecular geometry on the spectroscopic properties of the studied system, the extent to which we can control structural changes using pressure and the way it influences the emission properties, the role of intermolecular interactions, *etc.*

In order to answer these questions, at the beginning I carried out the TDDFT calculations at the DFT(PBE0)/LANL2DZ level of theory for isolated complex molecules in the ground-state geometry taken from the crystal structure and in the photocrystallographically-determined excited-state geometry. The evaluated UV-Vis absorption spectra suggested that if similar changes in the core geometry are achievable applying high pressure, there might be a chance to significantly affect the spectroscopic properties of the studied complex in this way. Encouraged by this illustrative data, I prepared research projects so as to apply for high-pressure X-ray diffraction measurements at the synchrotron, and for the possibility of conducting spectroscopic experiments in the corresponding pressure range. Both of my applications have been accepted. Thus, I conducted the former measurement with my team at the European Synchrotron

Radiation Facility (ESRF) in Grenoble, France, using the ID27 high-pressure beamline. Whereas, the high-pressure spectroscopic studies were realised at the LENS centre in Florence, Italy, during my 1.5-month stay as part of the Laserlab-Europe consortium facility-access programme.⁹

The synchrotron experiments were carried out up to a pressure of about 3.5 GPa due to progressive degradation of the sample by consecutive intense X-ray beam irradiation (the last low-quality measurement at 3.5 GPa is discussed in the article for illustrative purposes only). Although, in view of the above, determining the correct models of crystal structures under pressure presented a challenge, we achieved this goal thanks to very careful data processing and subsequent laborious refinements. In the applied model the ligand geometry was kept rigid, whereas the metal atoms, forming the most interesting for us core of the complex, were freely refined. In this way, we managed to evaluate crystal structures at five pressure points, *i.e.* 0.5, 1.0, 1.6, 2.2 and 3.5 GPa. In the last case we considered the model to be of lower quality, though.

At first, we analysed unit-cell parameters in the applied pressure range. It appeared that the crystal lattice constants, a , b and c , get shortened under increased pressure. In turn, the angles α and β begin to increase, reach the maximum between 1.6 and 2.2 GPa, and then decrease. The γ angle decreases with the elevated pressure (except for the last point). Although the described pressure-induced variations of unit-cell angles are rather small (about 1°), they are statistically significant. Furthermore, the non-monotonic behaviour of the angle values suggests that around 2 GPa we may expect some interesting changes in spectroscopic parameters and molecule's geometry. Despite these fluctuations, the unit cell undergoes gradual contraction with increasing pressure reaching at 3.5 GPa a volume of approximately 85% of that under atmospheric pressure. Additionally, we adapted the 3rd-order Birch-Murnaghan equation of state to our pressure data [129-130]. The result of the fit shows that the compressibility of the tested system is similar to that of aromatic hydrocarbon crystals, *e.g.* benzene [131], which is in line with our expectations, considering the nature of the majority of intermolecular interactions in the studied system.

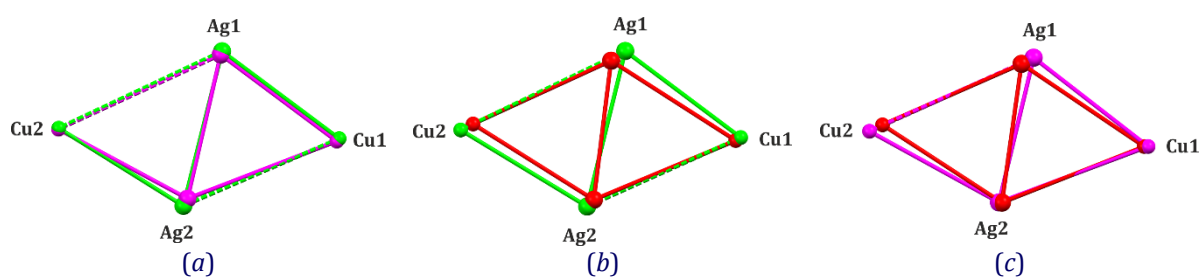


Figure 21. Overlay of metal cores of the $\text{Ag}_2\text{Cu}_2\text{L}_4$ complex: (a) ambient pressure & room temperature (green) vs. 2.7 GPa (magenta), (b) 90 K ground state (green) vs. excited state (red), (c) 2.7 GPa (magenta) vs. excited state (red). [Reprinted with permission from K. N. Jarzemska *et al.*, *Inorg. Chem.* **2018**, *57*, 8509. Copyright 2018 American Chemical Society.]

⁹ Synchrotron experiments at ID27 beamline [127] required using membrane high-pressure diamond-anvil cells (mDACs) in which the pressure can be controlled very precisely. Pressure inside the cell was monitored using the ruby crystal. In the case of LENS experiments the mDACs were also used, but the luminescence measurements were conducted in cells without ruby crystals (the ruby exhibits 'parasite' luminescence under the conditions of this particular experiment). In this case the pressure was monitored using the infrared spectroscopy – the shift of absorption bands of the sample under study was calibrated previously with independent measurement with mDAC with ruby crystal inside. The methodology of spectroscopic measurements is described in the literature in details [128].

In the next step, I compared the pressure-induced geometry changes of the complex core with those it experienced upon laser excitation. It appears that metal...metal contacts in both cases behave differently. Although the distance between the silver centres is reduced from 3.042(1) Å at the atmospheric pressure to 2.821(4) Å at 2.7 GPa, which undoubtedly suggests strengthening of the Ag–Ag bond, it is still substantially longer than that determined for the excited state (2.66(3) Å). In turn, the Ag...Cu contacts are affected in a more complex way. In particular, the Ag1–Cu1 and Ag2–Cu2 bonds at lower pressures shorten, while above 2 GPa they become longer. This observation is correlated with the changes of the unit-cell angles. The core geometries at different conditions are illustrated in Figure 21. I compared there the core shapes

in the complex structures determined at the atmospheric pressure, and at 2.7 GPa at room temperature, and in the ground-state and triplet excited-state complex structures measured at 90 K. The ‘zig-zag’ shape of the cluster centre seems to be maintained under high pressure, while the light excitation leads to its deformation towards a rhombus. These differences can partially be explained by intermolecular interactions in the crystal. As I have already mentioned in the article [H7], the complex fragments at the Cu1 and Cu2 sites differ from each other in this respect. The ligands attached to the Cu1 centre face the Cu1 site of the adjacent complex molecule in the crystal lattice, and the same applies to the Cu2 side of the studied species. In the case of light-induced excitation, the geometrical changes are more emphasised at the Cu2 site, which is involved in shorter contacts with the neighbouring molecule in the crystal when compared to the Cu1 equivalent. The charge transfer from the skatole ligands to the silver atoms significantly facilitates the shortening of the Ag–Ag bond, and generally, the core contraction due to the final charges on the silver centres being close to zero. In turn, during the hydrostatic compression, the Cu1 side of the molecule is deformed to a greater extent. This results from the fact that there is a slightly more ‘free’ space in the ground state around this part of the molecule (longer intermolecular interactions), which becomes the first thing to get reduced when the pressure increases. Different core deformation is also caused by smaller electron-density changes in the case of compression when compared to the effect of electronic excitation (the nature of both processes is substantially different). The impact of the increased hydrostatic pressure on both sides of the complex is illustrated by the respective Hirshfeld surfaces [132–134] (Figure 22). It is worth mentioning here that I also conducted theoretical calculations and carried out the QTAIM analysis of the resulting theoretical electron density distributions in the

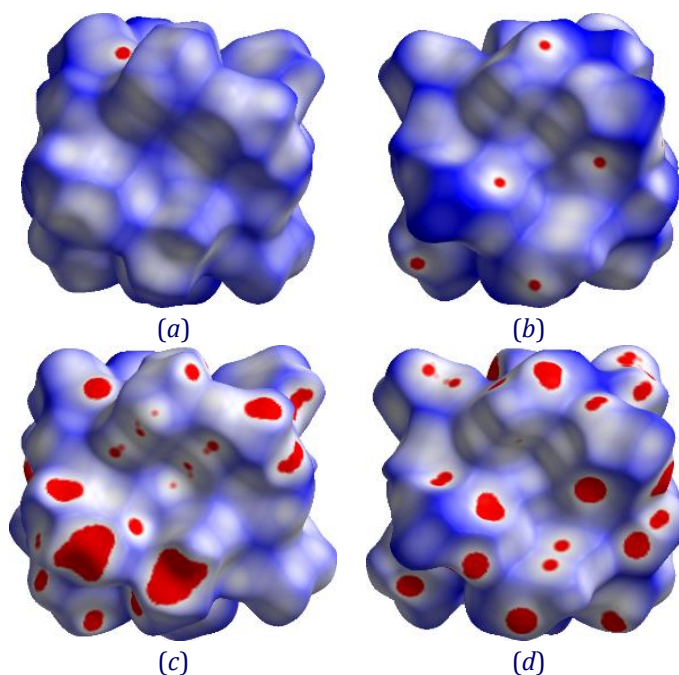


Figure 22. Hirshfeld surfaces with a d_{norm} property mapped generated for the room temperature ground state geometry of Ag₂Cu₂L₄ at ambient (top) and 2.7 GPa (bottom) pressure point. Left panels – the Cu1 side of the molecule, right – Cu2 side (in all cases view along Cu–Cu direction). [Reprinted with permission from K. N. Jarzemska *et al.*, *Inorg. Chem.* **2018**, *57*, 8509. Copyright 2018 American Chemical Society.]

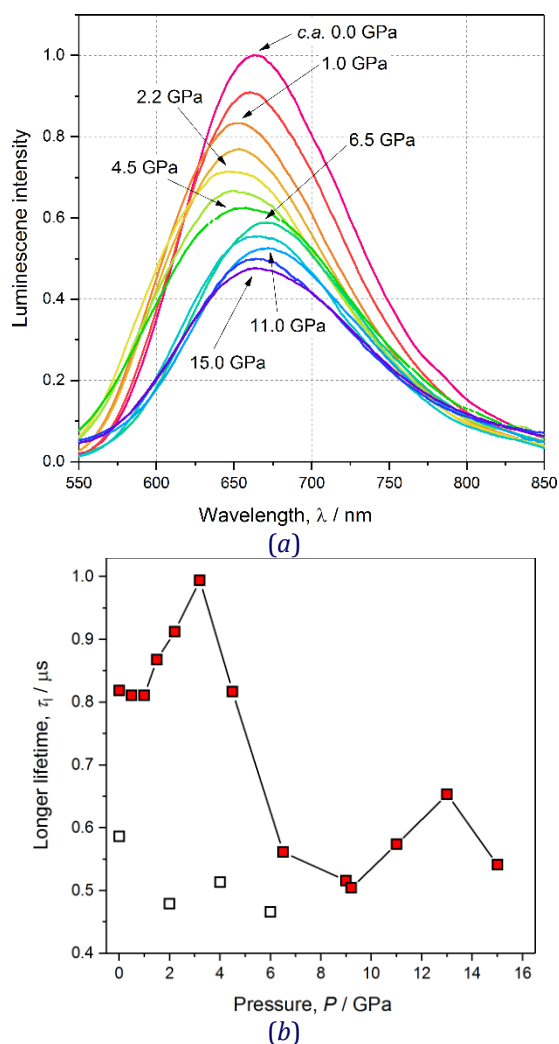


Figure 23. (a) Emission spectra of $\text{Ag}_2\text{Cu}_2\text{L}_4$ for various high-pressure points (spectra are shown with different heights for clarity). (b) Longer emission decay lifetime vs. pressure (full squares – compression, empty – decompression). [Reprinted with permission from K. N. Jarzemska *et al.*, *Inorg. Chem.* **2018**, *57*, 8509. Copyright 2018 American Chemical Society.]

rapidly decreases to about 0.5 μs remaining at this level irrespectively of further pressure changes (Figure 23b). The shorter decay time, which is not observed at atmospheric pressure, stays constant around 0.2(1) μs up to 15.0 GPa, and most probably corresponds to the formation of molecular fractions in the crystal, relaxation of which is determined by defects. Based on the above observations and outcomes, it can be concluded that the longer emission lifetime is correlated with the structural changes, while above 3.0 GPa molecular populations appear, relaxation of which is forced by crystal defects formed during compression. I also compared the spectroscopic results with the results of the TDDFT calculations, which I performed for an isolated molecule with geometries taken from the crystal structures under the applied pressure values. It turned out that even such a rough approximation reflects the experimental observations relatively well. Indeed, up to 2.2 GPa the absorption edge of the theoretical UV-Vis spectrum for the complex moiety shifts towards shorter wavelengths, while above this value it undergoes the red-shift.

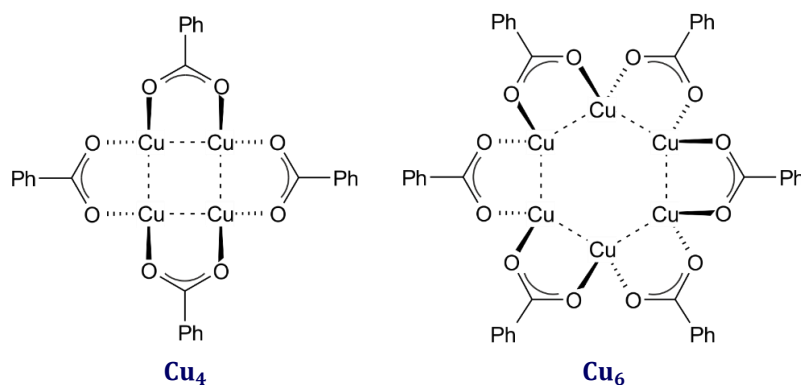
context of structural changes observed during the compression of the studied crystal structure. In this way, I assessed the nature of metallophilic interactions during crystal compression.

The second most important element of this work was the thorough examination of the spectroscopic properties of the studied complex crystals under elevated pressure. We collected the UV-Vis absorption and emission spectra of the tested system depending on the pressure, as well as, the emission lifetimes for each measurement. It turned out that in the case of the absorption edge it is well-defined and shifts to higher energies while the pressure is raised to approximately 2.6 GPa. Then the shift direction changes, and the spectrum becomes very spread. For the crystal emission similar behaviour is observed, *i.e.* up to about 3.0 GPa, the emission maximum shifts towards shorter wavelengths, and above this pressure, to about 6.5 GPa it gets red-shifted (Figure 23a). These changes are not fully reversible, which may be related to defects arising in the sample due to the lack of a hydrostatic medium. The emission decay can be considered as bi-exponential (*i.e.* $I(t) = A_1e^{-t/\tau_1} + A_2e^{-t/\tau_2}$), except at atmospheric pressure data, in which one exponential function was sufficient to model it. The longer of the determined phosphorescence lifetimes depends on the pressure and increases from about 0.8 μs to 1.0 μs at 4.0 GPa, and then

This study showed the complexity of the investigated phenomena. The shortening of the Ag–Ag bond, which is of great importance concerning the excited state nature, does not itself guarantee the expected emission red-shift. As it turned out, the contribution of copper atoms is crucial here, and the molecular environment has a significant influence on the complex deformation, in the case of both electronic excitation and compression. Nevertheless, we have received an agreement between the experimental results. It should also be noted that, although structural changes, and hence the spectroscopic properties cannot be fully controlled, the comprehensive analysis of the crystal structure allows to predict to some extent their character. At the time of publication, this work constituted the first literature report on the combined high-pressure crystallographic and spectroscopic studies performed for a coinage-metal complex in which metallophilic interactions are essential regarding the optical properties of the material.

[H9] Crystals, 2019, 9, 36. The last article from the presented series constitutes a continuation of the research which I presented in publications **[H7,H8]**, as well as my previous studies devoted to copper(I) complexes [102]. I decided to examine here two interesting systems based on copper(I) coordinated by carboxylate ligands, namely the tetranuclear complex $(\text{PhCO}_2)_4\text{Cu}_4$ (**Cu₄**) and its hexanuclear analogue $(\text{PhCO}_2)_6\text{Cu}_6$ (**Cu₆**). The choice of these compounds was dictated by the study of available literature. In the publication of Filatov *et al.* [135] the authors found that both of these compounds are luminescent and, additionally, a phase transition

takes place for the **Cu₆** crystal. Moreover, one compound can be transformed into another through sublimation and recrystallisation. The synthesis of the parent **Cu₄** system and its crystallisation was conducted by my colleague Wojciech



Scheme 6. Schematic representation of **Cu₄** and **Cu₆** complexes (Ph = phenyl).

Bury from the University of Wrocław. Schematic representation of both complexes is shown in Scheme 6.

I began analysing the systems by confirming their structure and performing spectroscopic measurements for single crystals of both **Cu₄** and **Cu₆** forms. It turned out that the **Cu₄** crystal shows luminescence thermochromism, which was not observed by the authors of the aforementioned article. The red emission band observed at room temperature (around 680 nm) gradually diminishes along with lowering temperature, while simultaneously the higher-energy green emission band (around 546 nm) appears (Figure 24). At a temperature of 200 K, the low-energy band is still more intense, but at 150 K, and below, the green emission predominates. The luminescence decay in both cases is well-represented by the biexponential function. The maximum of the high-energy band does not shift with temperature changes. In the case of the red emission, we observe a significant shift of the maximum towards higher energies when the temperature rises. All evaluated decay times significantly shorten when the sample is heated up from 90 K (Table 1). The microseconds decay times indicate phosphorescence. In the case of the **Cu₆** crystal, however, despite the phase transition in the system accompanied by a fairly

significant change of the crystal structure, practically no change in the emission spectrum is observed. The emission maximum shifts approximately by only 9 nm, when the temperature is increased from 90 K to 300 K. The phosphorescence decay time may also be well-described here by the bi-exponential function, but it is less affected by temperature changes than it was the case for the **Cu₄** crystals.

Therefore, I decided to quantify the effect which the temperature has on the crystal structures of both compounds. For that purpose, I conducted multi-temperature X-ray diffraction measurements for the studied systems. At first, I confirmed that the crystal of **Cu₆** undergoes a temperature-induced phase transition in the range of 253–263 K. In the case of the **Cu₄** crystal we did not observe this type of behaviour in the tested temperature range. The crystal structure of **Cu₄** contains two molecules of the complex in ASU (A and B). These two molecules differ substantially from each other regarding the geometrical parameters. The structure of the four-centre copper core of the complex is approximately parallelogram-shaped. Copper atoms, defining its shorter diagonal, are much closer together in the molecule A, than in B. In the first case this distance at 90 K is 2.8726(8) Å, which, according to standard criteria, can be considered as a metal–metal bond. In molecule B, the respective diagonal is longer than the sum of copper atom van der Waals radii (3.0797(9) Å). In both molecules, the parallelogram edges are indicated by cuprophilic interactions, which are on average shorter in molecule B. An important conclusion arising from the geometry analysis of the studied complexes is the observation that two symmetry-independent **Cu₄** molecules differ more significantly from each other regardless of temperature than the **Cu₆** particles before, or after phase transformation. In the case of the **Cu₆** molecules, there is no metal–metal bond along any diagonal of the core.

Luminescent thermochromism has already been observed for multi-centre copper compounds, but mainly for cubane-type-core complexes containing halogen atoms and organic ligands in their structure. The **Cu₄I₄(py)₄** (py = pyridine) system serves a good example here. Similarly to **Cu₄**, this complex exhibits two emission bands. The low-energy emission is

Table 1. The **Cu₄** complex solid-state luminescence lifetimes (τ) and emission peak maxima (λ_{em}) obtained from the least-squares fit at various temperatures (T). Letters “l” and “s” denote longer and shorter lifetime, respectively; “r” and “g” superscripts denote parameters for red- and green-light emission maxima, respectively.

T / K	$\tau_s^r / \mu s$	$\tau_l^r / \mu s$	λ_{em}^r / nm	$\tau_s^g / \mu s$	$\tau_l^g / \mu s$	λ_{em}^g / nm
90	11.6(3)	66.4(5)	718	15.3(4)	111.0(6)	547
150	5.2(1)	61.3(3)	682	10.4(2)	61.0(4)	546
200	2.5(3)	35.5(2)	673	5.4(1)	27.6(6)	546
250	2.13(4)	10.16(4)	668	–	–	–
RT	0.47(2)	1.65(2)	660	–	–	–

[136]. Most probably in the case of **Cu₄** we also deal with two emissive excited states, but surely

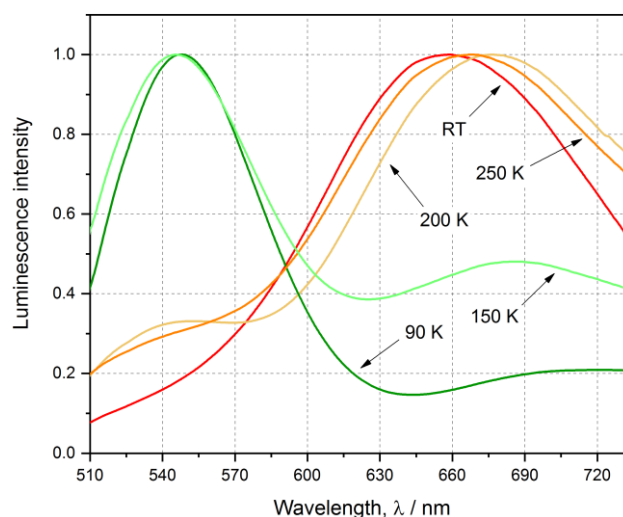


Figure 24. Emission spectra for the **Cu₄** single crystals collected at different temperatures.

attributed to the triplet excited state localised on the cluster core (³CC, cluster-centred), while the high-energy emission band is associated with the charge transfer from the halogen substituent to the ligand (³XLCT, halide-to-ligand charge transfer)

of a different nature. Moreover, for currently unknown reasons, the crystal of the related Cu_6 complex does not exhibit the luminescence thermochromism. Using my knowledge about the crystal structures of both compounds at different temperatures and the results of spectroscopic studies, in order to complete the picture and perhaps answer the questions that had arisen, I decided to perform theoretical modelling and photocrystallographic experiments. Theoretical calculations may help to understand the nature of the studied processes, determine possible electron transitions and their energy, and to estimate structural changes accompanying them, *etc.* The use of time-resolved Laue method would confirm whether at a given temperature we deal with the electron transition within the core of the molecule, or not, for example by observing its contraction under the influence of a light pulse.

Therefore, I invited my colleague Michał Hapka to cooperate, an expert in computational chemistry with experience in dealing with copper systems. M. Hapka performed a series of calculations, both for the isolated molecule of the examined complex and using the QM/MM approach, which are described in detail in the article. He applied the DFT method using the range separated functionals: CAM-B3LYP [137] and wB97XD [138]. The optimised isolated Cu_4 molecule exhibits the D_2 (or 222 in the international crystallographic notation) symmetry. This symmetry is reduced in the crystal structure due to intermolecular interactions, the impact of which is well-considered by the QM/MM method. It appeared that the two functionals provide very similar results. In addition, for both the isolated molecule and the molecule in the simulated crystal environment, comparable energies of the in successive excited states are obtained (Table 2). The first excited triplet state

Table 2. Lowest-energy triplet excited states computed for a single Cu_4 molecule for both isolated molecule (3rd column) and QM/MM results (4th and 5th columns).

No.	State	Method and Excitation energies / eV		
		CAM-B3LYP	QM/MM (mol. A)	QM/MM (mol. B)
1	1^3A	3.12	3.21	3.16
2	1^3B_1	3.27	3.32	3.35
3	1^3B_2	3.27	3.35	3.36
4	2^3A	3.28	3.36	3.37
5	1^3B_3	3.28	3.37	3.37
6	2^3B_1	3.32	3.39	3.46
7	2^3B_2	3.55	3.65	3.57
8	3^3A	4.12	4.12	4.14
9	2^3B_3	4.15	4.22	4.16
10	3^3B_1	4.23	4.26	4.23

(1^3A for a molecule of D_2 symmetry) involves transitions from HOMO, HOMO-1 and HOMO-2 orbitals to LUMO and several higher orbitals. The antibonding HOMO and bonding LUMO are localised majorly on copper atoms. This suggests that this electronic excited state is 3CC in nature. Just above this excited state there is a group of near-lying triplet states, three of which show the 3B symmetry and one 3A . The corresponding electronic transitions exhibit a ligand \rightarrow ligand and core \rightarrow ligand character. The analysis of the one-particle transition-density matrix (1-TDM) [139-141] showed that among the 10 lowest-energy electronic transitions evaluated for the Cu_4 complex there is a group of transitions centred on the complex core with a distinct MLCT contribution (states No. 1 and 6-9 in Table 2) and also a second group of excitations of predominant $\pi \rightarrow \pi^*$ character (states No. 2-5 in Table 2). To model the possible structural changes accompanying the excitation of a complex molecule to either one from the two emissive states, the two lowest-energy triplet states were optimised, namely the first triplet state T_1 and the subsequent triplet T_2 (corresponding to the 1st and 6th electronic states in Table 6). Both states T_1 and T_2 are of notable 3CC nature, thus, in both cases a significant contraction of the complex copper core is observed. The changes in the Cu...Cu distances are greater for T_1 , while for T_2 the Cu-O bonds are noticeably affected and get elongated. It should be mentioned that the convergence was not achieved for the $\pi \rightarrow \pi^*$ transitions, which should, however, lead mainly to deformations of the organic ligands. Energetic analysis of transitions from both triplet states to

the ground state showed that T_1 is most likely responsible for the low-energy (red) emission band. In turn, T_2 could be associated with the green emission. It should be noted here, however, that the results obtained for the isolated molecule does not reflect fully the situation in the crystal. Our analysis showed that for example the deformation of the molecule's geometry leads to a greater contribution of MLCT and LMCT transitions, at the expense of the 3CC character.

Photocrystallographic time-resolved measurements for the tested Cu_4 system using the Laue method constituted the next stage of the research. For this purpose, we conducted the laser-pump / X-ray-probe experiments at the APS synchrotron for single-crystal samples at two different temperatures: 90 and 225 K. Such experimental conditions were chosen based on the spectroscopic studies. At 90 K the green emission prevails, whereas at 225 K solely the low-energy band appears. The observation of any changes in the copper core geometry upon excitation, their character and degree, would help us to verify our theoretical predictions. We processed the measured data employing the available software [97,99], but also using our new method, which we recently implemented.¹⁰ Unfortunately, in this particular case, full refinement of the excited-state structure by means of the *LASER* program was not possible (due to the relatively low data completeness). Nevertheless, I managed to draw some qualitative

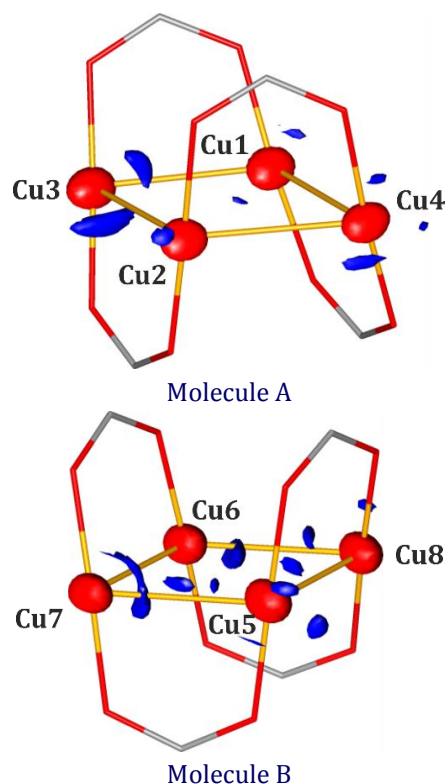


Figure 25. Photodifference maps drawn for the Cu_4 symmetry-independent molecules in ASU based on 90 K data (isosurfaces: $-2.0/+0.9 e \cdot \text{\AA}^{-3}$, blue colour – positive values, red – negative).

conclusions. The presence of negative peaks on the photodifference map (Figure 25) at the original copper atoms' positions suggests that these atoms could have possibly shifted when excited. In the case of both photodifference maps, *i.e.* at 90 K and 225 K, the respective patterns for the A and B molecules look almost identical, despite independently obtained samples being used, two different lasers, and also different reference monochromatic X-ray diffraction data sets. This indicates high reproducibility of experimental results, as well as the fact that most likely the same excited states were captured in both experiments. Comparing the nanosecond pump-probe delay (laser pulse to X-ray pulse time delay) with the microsecond decay times of the sample's emission, this explanation is by all means reasonable. The time between the probe and the pump pulses could have been shorter than the time needed for conversion of the populated excited state to the final emissive electronic state. Therefore, in both experiments we either sampled the singlet excited state, or higher

¹⁰ D. Szarejko, a student under my supervision, coded our new method of signal finding in the X-ray diffraction data using the C++ programming language. Our approach is based on the methods previously developed in P. Coppens' group – namely the analysis of 1-dimensional data sets collected with the area detector [97] and minimisation of the background intensity distribution skewness parameter [142]. The results are currently being prepared for publication and shall be extended by the parallel CUDA programming implementation. The new algorithm was used in the [H9] publication.

energetic triplet state, which is associated with the green emission. A more accurate analysis of the photodifference maps indicates that the core of the B molecule undergoes greater deformations upon laser irradiation (as suggested by the large peak at the Cu7 atom) than it is the case for the A molecule. This is most likely related to the fact that in the B molecule the shorter diagonal of the copper core is longer than that in the A species and it is subjected to greater contraction during excitation. Such observation is also supported by the QM/MM calculations for state T_1 .

Comparing, however, the computational results obtained for the Cu_6 complex molecule with those evaluated for Cu_4 , it is hard to find any significant differences that would indicate the presence of emission thermochromism, or its absence. Differences in the luminescent properties of these systems may be caused, for example, by a lower energy barrier between the two analysed emissive states for the Cu_6 complex, or by the crystal packing. We examined the latter option by conducting calculations for dimers composed of the closest adjacent molecules in both crystal structures. It turned out that indeed the first significant discrepancies appear for excited-state dimers. In the case of Cu_4 , excitations are localised on separate monomers, whereas for Cu_6 they are delocalised on both monomers forming exciton resonance states (without charge flow between the monomers). Such behaviour may lead to differences in emission properties of both complexes. Such delocalisation may, for example, enhance coupling between the excited states, leading to the observed low-energy emission band. Nevertheless, in order to evaluate the exact mechanism of these phenomena, it would be necessary to perform direct probing of excited-state dynamics and/or to examine the spectroscopic properties of isolated clusters, which is very difficult, if at all possible.

4.3.4. Summary

The presented series of publications, as a whole, cover structural, spectroscopic and photocrystallographic studies supported by theoretical modelling, leading to exploration of the nature of light-induced charge-transfer processes in new photoactive boron complexes and selected transition-metal systems. My most important achievements included in articles [H1-H9] are as follows:

- Explanation of the way in which water molecules may assemble by means of hydrogen bonds inside the channels of the porous *ortho*-phenylenediboronic acid crystal form, and quantification of these interactions [H1].
- Synthesis of the first luminescent boronic complexes, *i.e.* reaction products of *ortho*-phenylenediboronic acid and its fluorine derivatives with 8-hydroxyquinoline, and their comprehensive examination, including crystal-structure determination, analysis of equilibria present in the solution, investigations of the influence of boron atoms' acidity on the complex properties, evaluation of the spectroscopic properties, and verification of potential use of new compounds in the technology of organic luminescent diodes [H2].
- Determination of the solvent choice influence on the supramolecular structures formed by the photoactive complexes of *ortho*-phenylenediboronic acid with 8-hydroxyquinoline, and evaluation of their spectroscopic properties [H3].
- Experimental determination of the electron-density distribution in the crystal of the *ortho*-phenylenediboronic acid complex with 8-hydroxyquinoline containing 1,4-dioxane as a solvent, and correlating the parameters of this distribution with the calculated electronic transitions crucial in the context of spectroscopic properties of this system [H4].

- Demonstration that the *ortho*-phenylenediboronic acid complexes can be relatively easily formed with various (*N,O*)-donor ligands and their structural and spectroscopic analyses [H5]. Confirmation of the key role of the (*N,O*)-donor ligand in the context of the spectroscopic properties of the complex.
- Demonstration that it is possible to correlate the results of TDDFT calculations and the crystal structure of the new model photoactive complex $\text{Ti}_{17}\text{O}_{28}(\text{O}^i\text{Pr})_{16}\text{Fe}_2(\text{phen})_2$ (phen = 1,10-phenanthroline; ^iPr = isopropyl) with its photoelectrochemical properties [H6].
- Experimental determination of the short-lived excited-state structure of the model complex $\text{Ag}_2\text{Cu}_2\text{L}_4$ (L = 2-diphenylphosphino-3-methylindole) in the solid state and explaining the nature of the studied electronic transition [H7].
- Correlation of structural (molecule geometry) and spectroscopic (light emission) properties of the $\text{Ag}_2\text{Cu}_2\text{L}_4$ complex crystal subjected to high-pressure [H8]. Evaluation of the role of intermolecular interactions in the crystal structure, as an important factor affecting the structural changes observed upon light excitation and applied pressure.
- Observation of the luminescence thermochromism exhibited by the $(\text{PhCO}_2)_4\text{Cu}_4$ complex crystals and providing possible explanation of such behaviour based on wide set of results from both experimental (X-ray crystallography, solid-state spectroscopy, time-resolved X-ray Laue diffraction) and computational methods [H9]. Presentation of the hypothesis concerning the thermochromism of the $(\text{PhCO}_2)_4\text{Cu}_4$ system and its absence in the case of the $(\text{PhCO}_2)_6\text{Cu}_6$ analogue.
- Proposing of a new algorithm for finding signals in X-ray diffraction data based on statistical analysis.¹⁰

4.3.5. Research plans for the next few years

My plans for the upcoming years shall concern the research on functional photoactive materials. I plan to focus on studies of existing compounds with interesting spectral properties, in particular using (photo)crystallographic and spectroscopic methods supported by theoretical calculations, enabling acquiring in-depth knowledge and understanding of their structure and dynamics in solution and solid state during light irradiation. Based on the results of such analyses, I would like to design new functional materials in the future with potential applications, such as in optoelectronics. My plans assume both continuation of the research presented in this series, but also a number of new and already-started projects. The particular research perspectives are listed below:

- Studies of light-induced structural changes in transition-metal coordination complexes that undergo electronic excitations of different origins, such as LMCT, MLCT, or in particular – the most interesting – MMCT (metal-to-metal charge transfer), using the time-resolved photocystallographic methods. The project's intention is to correlate changes in the electronic structure of molecules with geometry deformations and to draw conclusions about the structure-property relationships. These processes are often very fast, so I intend to focus on the use of femtosecond methods in spectroscopy and photocystallography. These studies are / will be soon possible with the use of an X-ray free-electron laser (XFEL).
- Development of methodology of measurements and data processing for time-resolved photocystallography in order to increase its precision and accuracy. I intend, in particular, to extend the computer code we have created and to complement it with a graphical interface. These studies also include the evaluation of computational methods and algorithms on simulated and actual reference data collected on the synchrotron and using XFEL.

- Studies of intra- and intermolecular metallophilic interactions in crystals of coordination complexes of Cu, Ag, Au, Rh, Pt, *etc.*, and analyses of their impact on various properties of these systems (*e.g.* spectroscopic, magnetic, mechanic properties). Within the project I also intend to verify whether it is possible to control such properties via temperature or pressure changes.
- Continuation of the project dedicated to the research and design of photo-switchable materials, which I conduct within wide international cooperation. Together with my PhD student, we are currently studying a series of new systems which undergo the NO₂ group isomerisation upon light irradiation.

In my scientific activity I always do my best at approaching each research subject holistically and at combining the use of advanced experimental techniques with theoretical methodologies. In this context, global scientific cooperation often becomes vital for facilitating interdisciplinary research at the highest possible level and achieving the intended goals. I shall intend to continue this philosophy in my future research.

4.3.6. References

1. Grätzel, M., Recent advances in sensitized mesoscopic solar cells. *Acc. Chem. Res.* **2009**, *42*, 1788-1798.
2. Alibabaei, L., et al., Applications of metal oxide materials in dye sensitized photoelectrosynthesis cells for making solar fuels: let the molecules do the work *J. Mater. Chem. A* **2013**, *1*, 4133-4145.
3. Yersin, H., et al., The triplet state of organo-transition metal compounds. Triplet harvesting and singlet harvesting for efficient OLEDs. *Coord. Chem. Rev.* **2011**, *255*, 2622-2652.
4. Hall, D. G., *Boronic Acids: Preparation and Applications in Organic Synthesis, Medicine and Materials*. Wiley-VCH: 2011.
5. Miyaura, N.; Suzuki, A., Stereoselective synthesis of arylated (E)-alkenes by the reaction of alk-1-enylboranes with aryl halides in the presence of palladium catalyst. *J. Chem. Soc., Chem. Commun.* **1979**, 866-867.
6. Miyaura, N.; Suzuki, A., Palladium-catalyzed cross-coupling reactions of organoboron compounds. *Chem. Rev.* **1995**, *95*, 2457-2483.
7. Durka, M., et al., Dopamine/2-phenylethylamine sensitivity of ion-selective electrodes based on bifunctional-symmetrical boron receptors. *Sensors* **2019**, *19*, 283.
8. James, T. D., et al., *Boronic Acids in Saccharide Recognition*. The Royal Society of Chemistry: 2006.
9. Adamczyk-Wozniak, A., et al., ortho-(Aminomethyl)phenylboronic acids - synthesis, structure and sugar receptor activity *Appl. Organomet. Chem.* **2008**, *22*, 427.
10. Nishiyabu, R., et al., Boronic acid building blocks: tools for sensing and separation. *Chem. Commun.* **2010**, 1106-1123.
11. Wang, W., et al., Boronic acid-based sensors. *Curr. Org. Chem.* **2002**, *6*, 1285-1317.
12. Wade, C. R., et al., Fluoride ion complexation and sensing using organoboron compounds. *Chem. Rev.* **2010**, *110*, 3958-3984.
13. Yang, W., et al., Boronic acid compounds as potential pharmaceutical agents. *Med. Res. Rev.* **2003**, *23*, 346-368.
14. Adamczyk-Woźniak, A., et al., Diverse reactivity of 2-formylphenylboronic acid with secondary amines: synthesis of 3-amino-substituted benzoxaboroles. *Tetrahedron Lett.* **2010**, *51*, 6181-6183.
15. Jiong, Z., et al., The synthesis of benzoxaboroles and their applications in medicinal chemistry. *Sci. China Chem.* **2013**, *56*, 1372-1378.
16. Kettner, C.; Shenvi, A., Inhibition of the serine proteases leukocyte elastase, pancreatic elastase, cathepsin G, and chymotrypsin by peptide boronic acids. *J. Biol. Chem.* **1984**, *259*, 15106-15114.
17. Surolia, N., et al., Paradigm shifts in malaria parasite biochemistry and anti-malarial chemotherapy. *BioEssays* **2002**, *24*, 192-196.
18. Jabbour, A., et al., Synthesis and evaluation of oxazaborolidines for antibacterial activity against *Streptococcus mutans*. *J. Med. Chem.* **2004**, *47*, 2409-2410.
19. Adams, J., et al., Potent and selective inhibitors of the proteasome: dipeptidyl boronic acids. *Bioorg. Med. Chem. Lett.* **1998**, *8*, 333-338.
20. Barth, R. F., et al., Boron neutron capture therapy for cancer. *Sci. Am.* **1990**, *263*, 100-107.

21. Varughese, S., et al., Phenylboronic acids in crystal engineering: Utility of the energetically unfavorable syn,syn-conformation in co-crystal design. *Sci. China. Chem.* **2011**, *54*, 1909-1919.
22. Varughese, S., et al., Molecular complexes of alprazolam with carboxylic acids, boric acid, boronic acids, and phenols. evaluation of supramolecular heterosynthons mediated by a triazole ring. *J. Pharm. Sci.* **2010**, *99*, 3743-3753.
23. Najar, A. A.; Azim, Y., Pharmaceutical co-crystals: a new paradigm of crystal engineering. *J. Indian Inst. Sci.* **2014**, *94*, 45-67.
24. Anderson, S., et al., Materials for organic electroluminescence: aluminium vs. boron. *Synt. Met.* **2000**, *111-112*, 459-463.
25. Wesela-Bauman, G., et al., Heteroleptic (2-fluoro-3-pyridyl)arylboronic 8-oxyquinolates for the potential application in organic light-emitting devices. *Inorg. Chem.* **2013**, *52*, 10846-10859.
26. Wesela-Bauman, G., et al., Charge transfer properties of two polymorphs of luminescent (2-fluoro-3-pyridyl)(2,2'-biphenyl)boronic 8-oxyquinolate. *Phys. Chem. Chem. Phys.* **2014**, *16* (41), 22762-22774.
27. Durka, K., et al., Efficient 8-oxyquinolinato emitters based on a 9,10-dihydro-9,10-diboraanthracene scaffold for applications in optoelectronic devices. *J. Mater. Chem. C* **2015**, *3*, 1354-1364.
28. Qin, Y., et al., Luminescence tuning of organoboron quinolates through substituent variation at the 5-position of the quinolato moiety. *Org. Lett.* **2006**, *8*, 5227-5230.
29. Chai, J., et al., Synthesis and electrochemical properties of a new class of boron-containing n-type conjugated polymers. *Synth. Met.* **2009**, *159*, 1443-1449.
30. Januszewski, E., et al., Unsymmetrically substituted 9,10-Dihydro-9,10-diboraanthracenes as versatile building blocks for boron-doped π -conjugated systems. *Chem. Eur. J.* **2011**, *17*, 12696-12705.
31. Lorbach, A., et al., 9,10-Dihydro-9,10-diboraanthracene: supramolecular structure and use as a building block for luminescent conjugated polymers. *Angew. Chem. Int. Ed.* **2009**, *48*, 4584-4588.
32. Lorbach, A., et al., Lewis-base adducts of 9,10-dihydro-9,10-diboraanthracene: ditopic hydroboration reagents and a B-N analogue of triptycene. *Chem. Commun.* **2010**, *46*, 3592-3594.
33. Jäkle, F., Advances in the synthesis of organoborane polymers for optical, electronic, and sensory applications. *Chem. Rev.* **2010**, *110*, 3985-4022.
34. Chen, J., et al., Syntheses and structures of 6,13-dihydro-6,13-diborapentacenes: π -stacking in heterocyclic analogues of pentacene. *Organometallics* **2008**, *27*, 3639-3641.
35. Urban, M., et al., The effect of conformational isomerism on the optical properties of bis(8-oxyquinolato) diboron complexes with a 2,2'-biphenyl backbone. *Dalton Trans.* **2018**, *47*, 15670-15684.
36. Adamczyk-Woźniak, A., et al., Structure and properties of 1,3-phenylenediboronic acid: combined experimental and theoretical investigations. *Crystals* **2019**, *9*, 109.
37. Stewart, R. F., Electron population analysis with rigid pseudoatoms. *Acta Cryst. Sect. A* **1975**, *32*, 565-574.
38. Hansen, N. K.; Coppens, P., Testing aspherical atom refinements on small-molecule data sets. *Acta Cryst. Sect. A* **1978**, *34*, 909-921.
39. Coppens, P., *X-ray Charge Densities and Chemical Bonding*. International Union of Crystallography: 1997.
40. Domagała, S., et al., An improved experimental databank of transferable multipolar atom models - ELMAM2. Construction details and applications. *Acta Cryst.* **2012**, *A68*, 337-351.
41. Dittrich, B., et al., The generalized invariom database (GID). *Acta Cryst.* **2013**, *B69*, 91-104.
42. Sanjuan-Szklarz, W. F., et al., Yes, one can obtain better quality structures from routine X-ray data collection. *IUCrJ* **2016**, *3*, 61-70.
43. Spek, A. L., PLATON SQUEEZE: a tool for the calculation of the disordered solvent contribution to the calculated structure factors. *Acta Cryst. Sect. C* **2015**, *71*, 9-18.
44. Dovesi, R., et al., CRYSTAL: a computational tool for the ab initio study of the electronic properties of crystals. *Z. Kristallogr.* **2005**, *220*, 571-573.
45. Dovesi, R., et al. *CRYSTAL09*, University of Torino, Torino, Italy, 2009.
46. Durka, K., et al., Influence of fluorination and boronic group synergy on the acidity and structural behavior of *o*-phenylenediboronic acids. *Organometallics* **2014**, *33*, 1608-1616.
47. Liu, Y., et al., Deep-blue luminescent compound that emits efficiently both in solution and solid state with considerable blue-shift upon aggregation. *J. Mater. Chem. C* **2014**, *2*, 1068-1075.
48. Su, S., et al., Organic small-molecule materials for organic light-emitting diodes. In *Organic light-emitting materials and devices*, Li, Z. R., Ed. CRC Press / Taylor & Francis Group: Boca Raton, 2015; pp 309-487.

49. Gelbrich, T.; Hursthouse, M. B., A versatile procedure for the identification, description and quantification of structural similarity in molecular crystals. *CrystEngComm* **2005**, *7*, 324-336.
50. Gelbrich, T.; Hursthouse, M. B., Systematic investigation of the relationships between 25 crystal structures containing the carbamazepine molecule or a close analogue: a case study of the XPac method. *CrystEngComm* **2006**, *8*, 448-460.
51. Bader, R. F. W., *Atoms in Molecules: A Quantum Theory*. Clarendon Press: 1994.
52. Gillespie, R. J.; Popelier, P. L. A., *Chemical Bonding and Molecular Geometry: From Lewis to Electron Densities*. Oxford University Press: 2001.
53. Tsirelson, V. G.; Ozerov, R. P., *Electron Density and Bonding in Crystals: Principles, Theory and X-ray Diffraction Experiments in Solid State Physics and Chemistry*. CRC Press: 1996.
54. Matta, C. F., *Quantum Biochemistry*. Wiley-VCH: 2010.
55. Matta, C. F.; Boyd, R. J., *The Quantum Theory of Atoms in Molecules: From Solid State to DNA and Drug Design*. Wiley-VCH: 2007.
56. Durka, K., et al., On the nature of the B...N interaction and the conformational flexibility of arylboronic azaesters. *Phys. Chem. Chem. Phys.* **2010**, *12*, 13126-13136.
57. Nöth, H.; Wrackmeyer, B., *Nuclear Magnetic Resonance Spectroscopy of Boron Compounds*. Springer-Verlag Berlin Heidelberg: 1978.
58. Bertini, L., et al., Chemical insight into electron density and wave functions: software developments and applications to crystals, molecular complexes and materials science. *Theor. Chem. Acc.* **2007**, *117*, 847-884.
59. Gatti, C., et al., Crystal field effects on the topological properties of the electron density in molecular crystals: the case of urea. *J. Chem. Phys.* **1994**, *101*, 10686-10696.
60. Mebs, S., et al., Charge transfer via the dative N-B bond and dihydrogen contacts. Experimental and theoretical electron density studies of small Lewis acid-base adducts. *J. Phys. Chem. A* **2010**, *114*, 10185-10196.
61. Mebs, S., et al., Charge transfer via the dative N-B bond and dihydrogen contacts. Experimental and theoretical electron density studies of four deltahedral boranes. *J. Phys. Chem. A* **2011**, *115*, 1385-1395.
62. Chęcińska, L., et al., Tuning the electronic properties of the dative N-B bond with associated O-B interaction: electron localizability indicator from X-ray wavefunction refinement. *ChemPhysChem* **2016**, *17*, 1-13.
63. Torres-Huerta, A., et al., Structural induction via solvent variation in assemblies of triphenylboroxine and piperazine - potential application as self-assembly molecular sponge. *Cryst. Growth Des.* **2017**, *17*, 2438-2452.
64. Salazar-Mendoza, D., et al., Macrocycles and coordination polymers derived from self-complementary tectons based on N-containing boronic acids. *Cryst. Growth Des.* **2013**, *13*, 2441-2454.
65. Sheepwash, E., et al., Supramolecular polymers based on dative boron-nitrogen bonds. *Chem. Commun.* **2012**, *48*, 7808-7810.
66. Mallinson, P. R., et al., The Gram-Charlier and multipole expansions in accurate X-ray diffraction studies: can they be distinguished? *Acta Cryst. Sect. A* **1988**, *44*, 336-342.
67. Scheins, S., et al., Charge-density analysis of the ground state of a photochromic 1,10-phenanthroline zinc(II) bis(thiolate) complex. *Acta Cryst. Sect. B* **2010**, *66*, 366-372.
68. Meindl, K., et al., On the effect of neglecting anharmonic nuclear motion in charge density studies. *Acta Cryst. Sect. A* **2010**, *66*, 362-371.
69. Johnson, C. K., Addition of higher cumulants to the crystallographic structure-factor equation: a generalized treatment for thermal-motion effects. *Acta Cryst. Sect. A* **1969**, *25*, 187-194.
70. Kuhs, W. F., Statistical description of multimodal atomic probability densities. *Acta Cryst. Sect. A* **1983**, *39*, 148-158.
71. Scheringer, C., A deficiency of the cumulant expansion of the anharmonic temperature factor. *Acta Cryst. Sect. A* **1985**, *41*, 79-81.
72. Guillot, B., et al., Refinement of proteins at subatomic resolution with MoPro. *J. Appl. Cryst.* **2001**, *34*, 214-223.
73. Jelsch, C., et al., Advances in protein and small-molecule charge density refinement methods using MoPro. *J. Appl. Cryst.* **2005**, *38*, 38-54.
74. Mondal, S., et al., Experimental dynamic electron densities of multipole models at different temperatures. *Acta Cryst. Sect. A* **2012**, *68*, 568-581.
75. Dominiak, P. M., et al., Continua of interactions between pairs of atoms in molecular crystals. *Chem. Eur. J.* **2006**, *12*, 1941-1949.

76. Mallinson, P. R., et al., From weak interactions to covalent bonds: a continuum in the complexes of 1,8-bis(dimethylamino)naphthalene. *J. Am. Chem. Soc.* **2003**, *125*, 4259-4270.
77. Stasyuk, A. J., et al., Imidazo[1,2-a]pyridines susceptible to excited state intramolecular proton transfer: one-pot synthesis via an Ortoleva-King reaction. *J. Org. Chem.* **2012**, *77*, 5552-5558.
78. Coppens, P., et al., Crystallography of molecular excited states. Transition-metal nitrosyl complexes and the study of transient species. *J. Chem. Soc. Dalton Trans.* **1998**, 865-872.
79. Trzop, E.; Turowska-Tyrk, I., Monitoring structural transformations in crystals. 12. Course of an intramolecular [4 + 4] photocycloaddition in a crystal. *Acta Cryst. Sect. B* **2008**, *64*, 375-382.
80. Zheng, S.-L., et al., Single-crystal-to-single-crystal E to Z isomerization of tiglic acid in a supramolecular framework. *Acta Cryst. Sect. B* **2007**, *63*, 644-649.
81. Konieczny, K., et al., Structural transformations in crystals induced by radiation and pressure. Part 3. The pressure-induced structural changes versus the rate of the Norrish-Yang reaction in crystals. *J. Photochem. Photobiol. A* **2016**, *325*, 111-115.
82. Hatcher, L. E.; Raithby, P. R., Solid-state photochemistry of molecular photo-switchable species: the role of photocystallographic techniques. *Acta Cryst. Sect. C* **2013**, *69*, 1448-1456.
83. Hatcher, L. E.; Raithby, P. R., Dynamic single-crystal diffraction studies using synchrotron radiation. *Coord. Chem. Rev.* **2014**, *277-278*, 69-79.
84. Sylvester, S. O., et al., SO₂ phototriggered crystalline nanomechanical transduction of aromatic rotors in tosylates: rationalization via photocystallography of [Ru(NH₃)₄SO₂X]tosylate₂ (X = pyridine, 3-Cl-pyridine, 4-Cl-pyridine). *J. Phys. Chem. C* **2014**, *118*, 16003-16010.
85. Casaretto, N., et al., Photocystallography and IR spectroscopy of light-induced linkage NO isomers in [RuBr(NO)₂(PCyp₃)₂]BF₄. *Acta Cryst. Sect. B* **2015**, *71*, 788-797.
86. Warren, M. R., et al., Solid-state interconversions: unique 100% reversible transformations between the ground and metastable states in single-crystals of a series of nickel(II) nitro complexes. *Chem. Eur. J.* **2014**, *20*, 5468-5477.
87. Powers, D. C., et al., Photocystallographic observation of halide-bridged intermediates in halogen photoeliminations. *J. Am. Chem. Soc.* **2014**, *136*, 15346-15355.
88. Coppens, P., Molecular excited-state structure by time-resolved pump-probe X-ray diffraction. What is new and what are the prospects for further progress? *J. Phys. Chem. Lett.* **2011**, *2*, 616-621.
89. Coppens, P., et al., Time-resolved synchrotron diffraction and theoretical studies of very short-lived photo-induced molecular species. *Acta Cryst. Sect. A* **2010**, *66*, 179-188.
90. Graber, T., et al., BioCARS: a synchrotron resource for time-resolved X-ray science. *J. Synchrotron Rad.* **2011**, *18*, 658-670.
91. Wulff, M., et al., Realisation of sub-nanosecond pump and probe experiments at the ESRF. *Farad. Discuss.* **2002**, *122*, 13-26.
92. Fournier, B., et al., Analysis of multicrystal pump-probe data sets. II. Scaling of ratio data sets. *Acta Cryst. Sect. A* **2016**, *72*, 250-260.
93. Coppens, P.; Fournier, B., On the scaling of multicrystal data sets collected at high-intensity X-ray and electron sources. *Struct. Dyn.* **2015**, *2*, 064101.
94. Coppens, P.; Fournier, B., New methods in time-resolved Laue pump-probe crystallography at synchrotron sources. *J. Synchrotron Rad.* **2015**, *22*, 280-287.
95. Fournier, B.; Coppens, P., Analysis of multicrystal pump-probe data sets. I. Expressions for the RATIO model. *Acta Cryst. Sect. A* **2014**, *70*, 514-517.
96. Fournier, B.; Coppens, P., On the assessment of time-resolved diffraction results. *Acta Cryst. Sect. A* **2014**, *70*, 291-299.
97. Kalinowski, J. A., et al., The LaueUtil toolkit for Laue photocystallography. II. Spot finding and integration. *J. Synchrotron Rad.* **2012**, *19*, 637-646.
98. Makal, A., et al., The development of Laue techniques for single-pulse diffraction of chemical complexes: time-resolved Laue diffraction on a binuclear rhodium metal-organic complex. *Acta Cryst. Sect. A* **2011**, *67*, 319-326.
99. Kalinowski, J. A., et al., The LaueUtil toolkit for Laue photocystallography: I. Rapid orientation matrix determination for intermediate size unit-cell Laue data. *J. Appl. Cryst.* **2011**, *44*, 1182-1189.
100. Kamiński, R., et al., Optimizing the accuracy and precision of the single-pulse Laue technique for synchrotron photo-crystallography. *J. Synchrotron Rad.* **2010**, *17*, 479-485.
101. Coppens, P., et al., The RATIO method for time-resolved Laue crystallography. *J. Synchrotron Rad.* **2009**, *16*, 226-230.
102. Trzop, E., et al., Selective time-dependent changes of Cu(DPPE)(DMP)·PF₆ on photoexcitation. *Acta Cryst. Sect. A* **2014**, *70*, C776.

103. Makal, A., et al., Restricted photochemistry in the molecular solid state: structural changes on photoexcitation of Cu(I) phenanthroline metal-to-ligand charge transfer (MLCT) complexes by time-resolved diffraction. *J. Phys. Chem. A* **2012**, *116*, 3359-3365.
104. Collet, E., et al., Ultrafast spin-state photoswitching in a crystal and slower consecutive processes investigated by femtosecond optical spectroscopy and picosecond X-ray diffraction. *Phys. Chem. Chem. Phys.* **2012**, *14*, 6192-6199.
105. Benedict, J. B., et al., Time-resolved Laue diffraction of excited species at atomic resolution: 100 ps single-pulse diffraction of the excited state of the organometallic complex $\text{Rh}_2(\mu\text{-PNP})_2(\text{PNP})_2\cdot\text{BPh}_4$. *Chem. Commun.* **2011**, *47*, 1704-1706.
106. Kamtekar, K. T., et al., Recent advances in white organic light-emitting materials and devices (WOLEDs). *Adv. Mater.* **2010**, *22*, 572-582.
107. Yam, V. W.-W.; Lo, K. K.-W., Luminescent polynuclear d^{10} metal complexes. *Chem. Soc. Rev.* **1999**, *28*, 323-334.
108. Benedict, J. B.; Coppens, P., The crystalline nanocluster phase as a medium for structural and spectroscopic studies of light absorption of photosensitizer dyes on semiconductor surfaces. *J. Am. Chem. Soc.* **2010**, *132*, 2938-2944.
109. Benedict, J., et al., Large polyoxotitanate clusters: well-defined models for pure-phase TiO_2 structures and surfaces. *J. Am. Chem. Soc.* **2010**, *132*, 13669-13671.
110. Snoeberger III, R. C., et al., Interfacial electron transfer in functionalized polyoxotitanate nanocrystals. *J. Am. Chem. Soc.* **2012**, *134*, 8911-8917.
111. Sokolow, J. D., et al., Binding modes of carboxylate- and acetylacetonate-linked chromophores to homodisperse polyoxotitanate nanoclusters. *J. Am. Chem. Soc.* **2012**, *134*, 11695-11700.
112. Bao, J., et al., Excitons and excess electrons in nanometer size molecular polyoxotitanate clusters: electronic spectra, exciton dynamics, and surface states. *J. Phys. Chem. B* **2013**, *117*, 4422-4430.
113. Chen, Y., et al., Nanosized alkali-metal-doped ethoxotitanate clusters. *Inorg. Chem.* **2013**, *52*, 4750-4752.
114. Chen, Y., et al., A large manganese-doped polyoxotitanate nanocluster: $\text{Ti}_{14}\text{MnO}_{14}(\text{OH})_2(\text{OEt})_{28}$. *J. Chin. Chem. Soc.* **2013**, *60*, 887-890.
115. Wu, Y.-Y., et al., Metal-phenanthroline fused Ti_{17} clusters, a single molecular source for sensitized photoconductive films. *J. Mater. Chem. A* **2013**, *1*, 9862-9868.
116. Steunou, N., et al., A new polyoxo-alkoxo titanium cluster of the Keggin family: synthesis and characterization by X-ray diffraction and NMR spectroscopy. *J. Chem. Soc. Dalton Trans.* **1999**, 3653-3655.
117. Gratzel, M., Photoelectrochemical cells. *Nature* **2001**, *414*, 338-344.
118. Zheng, S.-L., et al., The nature of the $\text{Ag}^{\text{I}}\cdots\text{Ag}^{\text{I}}$ interaction in different $\text{Ag}(\text{NH}_3)_2$ dimers embedded in supramolecular solids. *Chem. Eur. J.* **2007**, *13*, 8583-8590.
119. Zheng, S.-L., et al., Ligand-unsupported Au(I) chains with short Au(I)...Au(I) contacts. *Chem. Commun.* **2006**, 3711-3713.
120. Coppens, P., et al., A very large Rh-Rh bond shortening on excitation of the $[\text{Rh}_2(1,8\text{-diisocyano-p-menthane})_4]^{2+}$ ion by time-resolved synchrotron X-ray diffraction. *Chem. Commun.* **2004**, 2144-2145.
121. Koshevoy, I. O., et al., Coinage metal complexes of 2-diphenylphosphino-3-methylindole. *Dalton Trans.* **2011**, *40*, 7927-7933.
122. Vorontsov, I., et al., LASER - a program for response-ratio refinement of time-resolved diffraction data. *J. Appl. Cryst.* **2010**, *43*, 1129-1130.
123. Schubert, H.; Wesemann, L., Silver dimer, tetramer, polymer, and network structures with the stannylene stanna-closo-dodecaborate. *Organometallics* **2010**, *29*, 4906-4913.
124. Catalano, V. J.; Malwitz, M. A., Short metal-metal separations in a highly luminescent trimetallic Ag(I) complex stabilized by bridging NHC ligands. *Inorg. Chem.* **2003**, *42*, 5483-5485.
125. Frisch, M. J., et al. *Gaussian 16*, Wallingford, CT, 2016.
126. Kamiński, R., et al., Constrained excited-state structure in molecular crystals by means of the QM/MM approach: toward the prediction of photocrystallographic results. *J. Phys. Chem. Lett.* **2010**, *1*, 2349-2353.
127. Mezouar, M., et al., Development of a new state-of-the-art beamline optimized for monochromatic single-crystal and powder X-ray diffraction under extreme conditions at the ESRF. *J. Synchrotron Rad.* **2005**, *12*, 659-664.
128. Citroni, M., et al., Crystalline indole at high pressure: chemical stability, electronic, and vibrational properties. *J. Phys. Chem. B* **2009**, *113*, 13526-13535.
129. Birch, F., Finite elastic strain of cubic crystals. *Phys. Rev.* **1947**, *71*, 809-824.

130. Gonzalez-Platas, J., et al., EosFit7-GUI: a new graphical user interface for equation of state calculations, analyses and teaching. *J. Appl. Cryst.* **2016**, *49*, 1377-1382.
131. Ciabini, L., et al., High-pressure and high-temperature equation of state and phase diagram of solid benzene. *Phys. Rev. B* **2005**, *72*, 094108.
132. Spackman, M. A.; Byrom, P. G., A novel definition of a molecule in a crystal. *Chem. Phys. Lett.* **1997**, *267*, 215-220.
133. Spackman, M. A.; Jayatilaka, D., Hirshfeld surface analysis. *CrystEngComm* **2009**, *11*, 19-32.
134. Spackman, M. A., Molecules in crystals. *Phys. Scr.* **2013**, *87*, 048103.
135. Filatov, A. S., et al., Reversible Cu₄ ↔ Cu₆ core interconversion and temperature induced single-crystal-to-single-crystal phase transition for copper(I) carboxylate. *Inorg. Chem.* **2010**, *49*, 1626-1633.
136. Ford, P. C., et al., Photoluminescence properties of multinuclear copper(I) compounds. *Chem. Rev.* **1999**, *99*, 3625-3647.
137. Yanai, T., et al., A new hybrid exchange-correlation functional using the Coulomb-attenuating method (CAM-B3LYP). *Chem. Phys. Lett.* **2004**, *393*, 51-57.
138. Chai, J. D.; Head-Gordon, M., Long-range corrected hybrid density functionals with damped atom-atom dispersion corrections. *Phys. Chem. Chem. Phys.* **2008**, *10*, 6615-6620.
139. Plasser, F.; Lischka, H., Analysis of excitonic and charge transfer interactions from quantum chemical calculations. *J. Chem. Theory Comput.* **2012**, *8*, 2777-2789.
140. Plasser, F.; Dreuw, A., High-level ab initio computations of the absorption spectra of organic iridium complexes. *J. Phys. Chem. A* **2015**, *119*, 1023-1036.
141. Tretiak, S.; Mukamel, S., Density matrix analysis and simulation of electronic excitations in conjugated and aggregated molecules. *Chem. Rev.* **2002**, *102*, 3171-3212.
142. Bolotovskiy, R., et al., The 'seed-skewness' method for integration of peaks on imaging plates. *J. Appl. Cryst.* **1995**, *28*, 86-95.

5. List of the remaining scientific publications

An asterisk (*) indicates the corresponding author; the impact factor (IF) is given for the year 2017 (the latest IF available in the Web of Science database); the number of citations (n.cit.) was taken from the Web of Science database (dated 6th March 2019); for each publication the initials of the names and surnames of the authors, the title of the article, the full name of the journal, publication year, volume number, page numbers and digital object identifier (DOI) are given; publications are grouped chronologically (the smaller the number the newer the paper).

↓ Publications **AFTER** PhD ↓

- P1.** L. Mazur,* J. Sączewski, **K. N. Jarzemska**, K. Szwarz-Karabyka, R. Paprocka, B. Modzelewska-Banachiewicz, "Synthesis, structural characterization and reactivity of new trisubstituted *N*¹-acylamidrazones: solid state and solution studies", *CrystEngComm*, **2018**, *20*, 4179-4193 (DOI: 10.1039/C8CE00701B).
(IF₂₀₁₇ = 3.304; n.cit. = 0)
- P2.** **K. N. Jarzemska**,* A. A. Hoser, S. Varughese, R. Kamiński, M. Malinska, M. Stachowicz, V. R. Pedireddi, K. Woźniak,* "Structural and energetic analysis of molecular assemblies in the series of nicotinamide and pyrazinamide cocrystals with dihydroxybenzoic acids", *Crystal Growth & Design*, **2017**, *17*, 4918-4931 (DOI: 10.1021/acs.cgd.7b00868).
(IF₂₀₁₇ = 3.972; n.cit. = 5)
- Virtual special issue honoring Prof. William Jones and His contributions to organic solid-state chemistry**
- P3.** **K. N. Jarzemska**,* K. Ślepokura, R. Kamiński, M. J. Gutmann, P. M. Dominiak, K. Woźniak, "Multi-temperature study of potassium uridine-5'-monophosphate: electron density distribution and anharmonic motion modelling", *Acta Crystallographica Section B*, **2017**, *73*, 550-564 (DOI: 10.1107/S2052520617005534).
(IF₂₀₁₇ = 6.467; n.cit. = 2)
- Special issue entitled "Charge density and photo-/time-resolved crystallography: a tribute to Professor Philip Coppens"**
- P4.** M. Wilk-Kozubek,* **K. N. Jarzemska**, J. Janczak, V. Videnova-Adrabska,* "Synthesis, structural characterization and computational studies of catena-poly[chlorido-[μ₃-(pyridin-1-ium-3-yl)phosphonato-κ³O:O':O'']zinc(II)]", *Acta Crystallographica Section C*, **2017**, *73*, 363-368 (DOI: 10.1107/S2053229617004478).
(IF₂₀₁₇ = 8.678; n.cit. = 0)
- P5.** L. Mazur,* A. E. Koziol, **K. N. Jarzemska**, R. Paprocka, B. Modzelewska-Banachiewicz, "Polymorphism and isostructurality of the series of 3-(4,5-diaryl-4*H*-1,2,4-triazole-3-yl)propenoic acid derivatives", *Crystal Growth & Design*, **2017**, *17*, 2104-2115 (DOI: 10.1021/acs.cgd.7b00080).
(IF₂₀₁₇ = 3.972; n.cit. = 7)
- P6.** P. Coppens,* A. Makal, B. Fournier, **K. N. Jarzemska**, R. Kamiński, K. Basuroy, E. Trzop, "A priori checking of the light-response and data quality before extended data collection in pump-probe photocrystallography experiments", *Acta Crystallographica Section B*, **2017**, *73*, 23-26 (DOI: 10.1107/S2052520616017558).
(IF₂₀₁₇ = 6.467; n.cit. = 2)

- P7.** S. E. Kutyla, D. K. Stępień,* **K. N. Jarzemska,*** R. Kamiński, Ł. Dobrzycki, A. Ciesielski, R. Boese, J. Młochowski, M. K. Cyrański,* “Structural and stability studies of a series of *para*-phenylenediboronic and *para*-hydroxyphenylboronic acid cocrystals with selected aromatic *N*-oxides”, *Crystal Growth & Design*, **2016**, *16*, 7037-7050 (DOI: 10.1021/acs.cgd.6b01250).
(IF₂₀₁₇ = 3.972; n.cit. = 5)
- P8.** R. Kamiński,* **K. N. Jarzemska,*** S. E. Kutyla, M. Kamiński, “A portable light-delivery device for *in situ* photocrystallographic experiments at home laboratory. *Journal of Applied Crystallography*, **2016**, *49*, 1383-1387 (DOI: 10.1107/S1600576716008128).
(IF₂₀₁₇ = 3.422; n.cit. = 3)
- P9.** L. Mazur,* **K. N. Jarzemska**, R. Kamiński, A. A. Hoser, A. Ø. Madsen, E. Pindelska, M. Zielińska-Pisklak, “Crystal structures and thermodynamic properties of polymorphs and hydrates of selected 2-pyridinecarboxaldehyde hydrazones”, *Crystal Growth & Design*, **2016**, *16*, 3101-3112 (DOI: 10.1021/acs.cgd.5b01673).
(IF₂₀₁₇ = 3.972; n.cit. = 6)
- P10.** Y. Chen, **K. N. Jarzemska**, E. Trzop, P. Coppens,* “Reply to: How does substitutional doping affect visible light absorption in a series of homodisperse Ti₁₁ polyoxotitanate nanoparticles – a comment on the band gap determination of the Fe^{II} cages”, *Chemistry – A European Journal*, **2016**, *22*, 4634-4636 (DOI: 10.1002/chem.201600041).
(IF₂₀₁₇ = 5.160; n.cit. = 0)
- P11.** R. Kamiński,* **K. N. Jarzemska,*** M. Dąbrowski, K. Durka, M. Kubsik, J. Serwatowski, K. Woźniak, “Finding rules governing layered architectures of trifluoroborate potassium salts in the solid state”, *Crystal Growth & Design*, **2016**, *16*, 1687-1700 (DOI: 10.1021/acs.cgd.5b01760).
(IF₂₀₁₇ = 3.972; n.cit. = 6)
- P12.** P. Coppens,* L. Zhang, R. Thomas, Y. Chen, **K. Jarzemska**, R. Kaminski, E. Trzop, B. Fournier, “Can we deconvolute electron density changes from the dominant influence of the atomic rearrangement on molecular excitation in time-resolved diffraction studies?”, *Physica Scripta*, **2016**, *91*, 023003 (DOI: 10.1088/0031-8949/91/2/023003).
(IF₂₀₁₇ = 1.902; n.cit. = 0)
- Invited comment in focus issue on charge, spin and momentum densities: SAGAMORE XVIII**
- P13.** Y. Chen, **K. N. Jarzemska**, E. Trzop, L. Zhang, P. Coppens,* “How does substitutional doping affect visible light-absorption in a series of homodisperse Ti₁₁ polyoxotitanate nanoparticles?”, *Chemistry – A European Journal*, **2015**, *21*, 11538-11544 (DOI: 10.1002/chem.201500961).
(IF₂₀₁₇ = 5.160; n.cit. = 18)
- P14.** S. Varughese,* A. A. Hoser,* **K. N. Jarzemska**, V. R. Pedireddi, K. Woźniak, “Positional isomerism and conformational flexibility directed structural variations in the molecular complexes of dihydroxybenzoic acids”, *Crystal Growth & Design*, **2015**, *15*, 3832-3841 (DOI: 10.1021/acs.cgd.5b00471).
(IF₂₀₁₇ = 3.972; n.cit. = 6)

- P15.** K. N. Jarzemska,* R. Kamiński, Ł. Dobrzycki,* M. K. Cyrański, "First experimental charge density study using a Bruker CMOS-type PHOTON 100 detector: the case of ammonium tetraoxalate dihydrate. Addendum", *Acta Crystallographica Section B*, **2015**, *71*, 241-243 (DOI: 10.1107/S2052520615001146).
(IF₂₀₁₇ = 6.467; n.cit. = 3)
- P16.** M. Wilk,* K. N. Jarzemska, J. Janczak, M. Duczmal, J. Hoffmann, V. Videnova-Adrabska,* "Synthesis, structural characterization and computational studies of layered metal phosphonates: [M(HO₃P-C₅H₄N-PO₃H)₂(H₂O)₂]_n [M^{II} = Co, Zn, Cd]", *RSC Advances*, **2014**, *4*, 58858-58866 (DOI: 10.1039/C4RA10257F).
(IF₂₀₁₇ = 2.936; n.cit. = 5)
- P17.** C. F. A. Negre, K. J. Young, M. Belén Oviedo, L. J. Allen, C. G. Sánchez, K. N. Jarzemska, J. B. Benedict, R. H. Crabtree, P. Coppens,* G. W. Brudvig,* V. S. Batista,* "Photoelectrochemical hole injection revealed in polyoxotitanate nanocrystals functionalized with organic adsorbates", *Journal of the American Chemical Society*, **2014**, *136*, 16420-16429 (DOI: 10.1021/ja509270f).
(IF₂₀₁₇ = 14.357; n.cit. = 31)
- P18.** K. N. Jarzemska,* R. Kamiński, Ł. Dobrzycki,* M. K. Cyrański, "First experimental charge density study using a Bruker CMOS-type PHOTON 100 detector: the case of ammonium tetraoxalate dihydrate", *Acta Crystallographica Section B*, **2014**, *70*, 847-855 (DOI: 10.1107/S2052520614017570).
(IF₂₀₁₇ = 6.467; n.cit. = 6)
- P19.** M. Wilk,* K. N. Jarzemska, J. Janczak, J. Hoffman, V. Videnova-Adrabska,* "Synthesis, crystal structure and computational studies of 4-nitrobenzylphosphonic acid", *Journal of Molecular Structure*, **2014**, *1074*, 240-249 (DOI: 10.1016/j.molstruc.2014.05.052).
(IF₂₀₁₇ = 2,011; n.cit. = 8)
- P20.** K. N. Jarzemska, A. A. Hoser, R. Kamiński,* A. Ø. Madsen, K. Durka, K. Woźniak, "Combined experimental and computational studies of pyrazinamide and nicotinamide in the context of crystal engineering and thermodynamics", *Crystal Growth & Design*, **2014**, *14*, 3453-3465 (DOI: 10.1021/cg500376z).
(IF₂₀₁₇ = 3.972; n.cit. = 22)
- P21.** L. Mazur,* K. N. Jarzemska, R. Kamiński, K. Woźniak, E. Pindelska, M. Zielińska-Pisklak, "Substituent and solvent effects on intermolecular interactions in crystals of *N*-acylhydrazones derivatives: single-crystal X-ray, solid-state NMR and computational studies", *Crystal Growth & Design*, **2014**, *14*, 2263-2281 (DOI: 10.1021/cg401866x).
(IF₂₀₁₇ = 3.972; n.cit. = 17)
- P22.** P. Kumar, S. Bojarowski, K. N. Jarzemska, S. Domagała, K. Vanommeslaeghe, A. MacKerell Jr., P. M. Dominiak,* "A comparative study of transferable aspherical pseudoatom databank and classical force fields for predicting electrostatic interactions in molecular dimers", *Journal of Chemical Theory and Computation*, **2014**, *10*, 1652-1664 (DOI: 10.1021/ct4011129).
(IF₂₀₁₇ = 5.399; n.cit. = 9)

P23. A. Poulain, E. Wenger, P. Durand, **K. N. Jarzemska**, R. Kamiński, P. Fertey, M. Kubicki,* C. Lecomte,* “Anharmonicity and isomorphic phase transition: a multi-temperature X-ray single crystal and powder diffraction study of 1-(2'-aminophenyl)-2-methyl-4-nitroimidazole”, *IUCrj*, **2014**, *1*, 110-118 (DOI: 10.1107/S2052252514002838).

(IF₂₀₁₇ = 6.544; n.cit. = 10)

P24. M. Malińska,* **K. N. Jarzemska**, A. M. Goral, A. Kutner, K. Woźniak, P. M. Dominiak,* “Sunitinib: from charge-density studies to interaction with proteins”, *Acta Crystallographica Section D*, **2014**, *70*, 1257-1270 (DOI: 10.1107/S1399004714002351).

(IF₂₀₁₇ = 3.099; n.cit. = 18)

P25. K. Durka,* S. Luliński, **K. N. Jarzemska**, J. Smętek, J. Serwatowski, K. Woźniak,* “Competition between hydrogen and halogen bonding in the structures of 5,10-dihydroxy-5,10-dihydroboranthrenes”, *Acta Crystallographica Section B*, **2014**, *70*, 157-171 (DOI: 10.1107/S2052520613034987).

(IF₂₀₁₇ = 6.467; n.cit. = 16)

Special issue entitled “Crystal Engineering”

P26. R. Kamiński,* S. Domagała,* **K. N. Jarzemska**, A. A. Hoser, W. F. Sanjuan-Szklarz, M. J. Gutmann, A. Makal, M. Malińska, J. M. Bąk, K. Woźniak, “Statistical analysis of multipole-model-derived structural parameters and charge-density properties from high-resolution X-ray diffraction experiments”, *Acta Crystallographica Section A*, **2014**, *70*, 72-91 (DOI: 10.1107/S2053273313028313).

(IF₂₀₁₇ = 7.930; n.cit. = 27)

P27. **K. N. Jarzemska**,* R. Kamiński, E. Wenger, C. Lecomte, P. M. Dominiak, “Interplay between charge density distribution, crystal structure energetic features, and crystal morphology of 6-methyl-2-thiouracil”, *Journal of Physical Chemistry C*, **2013**, *117*, 7764-7775 (DOI: 10.1021/jp312158m).

(IF₂₀₁₇ = 4.484; n.cit. = 20)

P28. R. Kamiński,* **K. N. Jarzemska**, S. Domagała, “CLUSTERGEN: a program for molecular cluster generation from crystallographic data”, *Journal of Applied Crystallography*, **2013**, *46*, 540-534 (DOI: 10.1107/S0021889813002173).

(IF₂₀₁₇ = 3.422; n.cit. = 20)

P29. **K. N. Jarzemska**,* A. M. Goral, R. Gajda, P. M. Dominiak,* “Hoogsteen-Watson-Crick 9-methyladenine:1-methylthymine complex: charge density study in the context of crystal engineering and nucleic acid base pairing”, *Crystal Growth & Design*, **2013**, *13*, 239-254 (DOI: 10.1021/cg301393e).

(IF₂₀₁₇ = 3.972; n.cit. = 13)

↑ Publications **AFTER** PhD



↓ Publications **BEFORE** PhD



P30. A. A. Hoser, **K. N. Jarzemska**, Ł. Dobrzycki, M. J. Gutmann, K. Woźniak,* “Differences in charge density distribution and stability of two polymorphs of benzidine dihydrochloride”, *Crystal Growth & Design*, **2012**, *12*, 3526-3539 (DOI: 10.1021/cg300337a).

(IF₂₀₁₇ = 3.972; n.cit. = 22)

- P31.** K. Durka,* **K. N. Jarzemska**, R. Kamiński, S. Luliński, J. Serwatowski, K. Woźniak,* “Structural and energetic landscape of fluorinated 1,4-phenylenediboronic acids”, *Crystal Growth & Design*, **2012**, *12*, 3720-3734 (DOI: 10.1021/cg3005272).
(IF₂₀₁₇ = 3.972; n.cit. = 44)
- Virtual special issue entitled “In honor of Prof. Gautam R. Desiraju”**
- P32.** **K. N. Jarzemska**,* M. Kubsik, R. Kamiński, K. Woźniak, P. M. Dominiak,* “From a single molecule to molecular crystal architectures: structural and energetic studies of selected uracil derivatives”, *Crystal Growth & Design*, **2012**, *12*, 2508-2524 (DOI: 10.1021/cg300129z).
(IF₂₀₁₇ = 3.972; n.cit. = 38)
- P33.** **K. N. Jarzemska**, D. Kamiński, A. A. Hoser, M. Malińska, B. Senczyna, K. Woźniak,* M. Gagoś,* “Controlled crystallization, structure, and molecular properties of iodoacetylamphtericin B”, *Crystal Growth & Design*, **2012**, *12*, 2336-2345 (DOI: 10.1021/cg2017227).
(IF₂₀₁₇ = 3.972; n.cit. = 22)
- P34.** **K. N. Jarzemska**,* P. M. Dominiak,* “New version of the theoretical databank of transferable aspherical pseudoatoms, UBDB2011 – towards nucleic acid modelling”, *Acta Crystallographica Section A*, **2012**, *68*, 139-147 (DOI: 10.1107/S0108767311042176).
(IF₂₀₁₇ = 7.930; n.cit. = 53)
- P35.** A. Szadkowska, X. Gstrein, D. Burtscher, **K. Jarzemska**, K. Woźniak, C. Slugovc,* K. Grell,* “Latent thermo-switchable olefin metathesis initiators bearing a pyridyl-functionalized chelating carbene: influence of the leaving group’s rigidity on the catalyst’s performance”, *Organometallics*, **2010**, *29*, 117-124 (DOI: 10.1021/om900857w).
(IF₂₀₁₇ = 4.051; n.cit. = 47)
- P36.** Ż. Czyżnikowska,* R. W. Góra, R. Zalesny, P. Lipkowski, **K. N. Jarzemska**, P. M. Dominiak, J. Leszczynski, “Structural variability and the nature of intermolecular interactions in Watson-Crick B-DNA base pairs”, *Journal of Physical Chemistry B*, **2010**, *114*, 9629-9644 (DOI: 10.1021/jp101258q).
(IF₂₀₁₇ = 3.146; n.cit. = 26)
- P37.** **K. Jarzemska**, S. Seal, K. Woźniak,* A. Szadkowska, M. Bieniek, K. Grell,* “X-ray photoelectron spectroscopy and reactivity studies of a series of ruthenium catalysts”, *ChemCatChem*, **2009**, *1*, 144-151 (DOI: 10.1002/cctc.200900052).
(IF₂₀₁₇ = 4.674; n.cit. = 8)
- P38.** P. M. Dominiak,* A. Volkov, A. P. Dominiak, **K. N. Jarzemska**, P. Coppens,* “Combining crystallographic information and an aspherical-atom data bank in the evaluation of the electrostatic interaction energy in an enzyme-substrate complex: influenza neuraminidase inhibition”, *Acta Crystallographica Section D*, **2009**, *65*, 485-499 (DOI: 10.1107/S0907444909009433).
(IF₂₀₁₇ = 3.099; n.cit. = 33)

IUCr Highlight

P39. M. Barbasiewicz,* A. Szadkowska, A. Makal, **K. Jarzemska**, K. Woźniak, K. Grela,* “Is the Hoveyda-Grubbs complex a vinylogous Fischer-type carbene? Aromaticity-controlled activity of ruthenium metathesis catalysts”, *Chemistry – A European Journal*, **2008**, *14*, 9330-9337 (DOI: 10.1002/chem.200800704).

(IF₂₀₁₇ = 5.160; n.cit. = 42)

P40. M. Bieniek, R. Bujok, H. Stępowaska, A. Jacobi, R. Hagenkötter, D. Arlt,* **K. Jarzemska**, A. Makal, K. Woźniak, K. Grela,* “New air-stable ruthenium olefin metathesis precatalysts derived from bisphenol S”, *Journal of Organometallic Chemistry*, **2006**, *691*, 5289-5297 (DOI: 10.1016/j.jorganchem.2006.07.041).

(IF₂₀₁₇ = 1.946; n.cit. = 24)

Special issue entitled “Transition Metal Mediated Metathesis”



Publications **BEFORE** PhD



*Scientometric data of the **entire** scientific output (i.e. together with [H1-H9] contributions):* ^{iv}

No. of research publications: **49**

Total number of citations (without self-citations): **696 (539)**

Total impact factor (IF): **228.249 (4.658 average per paper)**

Hirsh index (IH): **18**

Katarzyna N. Jarzemska